A comprehensive global three-dimensional model of $\delta^{18}O$ in atmospheric CO_2: 2. Mapping the atmospheric signal

Matthias Cuntz, Philippe Ciais, Georg Hoffmann, Colin E. Allison, Roger J. Francey, Wolfgang Knorr, Pieter P. Tans, James W. C. White, Ingeborg Levin

▶ **To cite this version:**

Matthias Cuntz, Philippe Ciais, Georg Hoffmann, Colin E. Allison, Roger J. Francey, et al.. A comprehensive global three-dimensional model of $\delta^{18}O$ in atmospheric CO_2: 2. Mapping the atmospheric signal. Journal of Geophysical Research, 2003, 108 (D17), pp.4528. 10.1029/2002JD003154 . hal-02681705

HAL Id: hal-02681705
https://hal.inrae.fr/hal-02681705

Submitted on 18 Jul 2021

HAL is a multi-disciplinary open access archive for the deposit and dissemination of scientific research documents, whether they are published or not. The documents may come from teaching and research institutions in France or abroad, or from public or private research centers.

L'archive ouverte pluridisciplinaire **HAL**, est destinée au dépôt et à la diffusion de documents scientifiques de niveau recherche, publiés ou non, émanant des établissements d'enseignement et de recherche français ou étrangers, des laboratoires publics ou privés.

Copyright

JOURNAL OF GEOPHYSICAL RESEARCH, VOL. 108, NO. D17, 4528, doi:10.1029/2002JD003154, 2003

A comprehensive global three-dimensional model of $\delta^{18}O$ in atmospheric CO_2: 2. Mapping the atmospheric signal

Matthias Cuntz,[1,2] Philippe Ciais,[1] Georg Hoffmann,[1] Colin E. Allison,[3] Roger J. Francey,[3] Wolfgang Knorr,[4] Pieter P. Tans,[5] James W. C. White,[6] and Ingeborg Levin[2]

Received 7 November 2002; revised 1 March 2003; accepted 1 May 2003; published 4 September 2003.

[1] We have modeled the distribution of $\delta^{18}O$ in atmospheric CO_2 with a new comprehensive global three-dimensional model. We have focused in this study on the seasonal cycle and the meridional gradient in the atmosphere. The model has been compared with a data set of $\delta^{18}O$-CO_2, which merges measurements made by different laboratories, with allowance for recently elucidated calibration biases. The model compares well with the seasonal cycle of CO_2, but advances the measured $\delta^{18}O$-CO_2 seasonal cycle by two months. The calculated seasonal amplitude is typically 2/3 of the measured value, but the sensitivity to uncertainties in the input parameter set is such that a range of amplitudes over a factor of 3 is accommodated. Unlike the case for the amplitude, the sensitivity analyses demonstrate that the modeled phase of the seasonal cycle and the north-south gradient are practically unaffected by uncertainty in the parameter set. The north-south gradient comes, on the one hand, from the disequilibrium of the $\delta^{18}O$-CO_2 isofluxes at every grid point and, on the other hand, from rectification gradients, a covariance of the varying $\delta^{18}O$-CO_2 source with the atmospheric transport. The model exhibits a very strong rectification gradient that can lead to a misinterpretation of the measurements compared to the model. We therefore restrict comparison to the latitudinal means of only ocean grid cells with measurements from stations sampling the marine boundary layer. Assimilation and respiration are the determining factors of the seasonal cycle and the north-south gradient of $\delta^{18}O$-CO_2. In a number of sensitivity studies we have explored the range of possible processes affecting the simulated seasonal cycle and hemispheric gradient. None of these processes contributed significantly to improve the model-observation mismatch. The contribution of assimilation and respiration to the total signal does change significantly in the sensitivity studies, but, because of feedback processes, they change in such a way that the overall response of the model is only marginally altered. In particular, prescribing $\delta^{18}O$-H_2O soil values to monthly means of rain does not significantly change the modeled signal, either in the seasonal cycle or in the meridional gradient. This highlights the need to accurately model assimilation and respiration in order to understand $\delta^{18}O$ in atmospheric CO_2. *INDEX TERMS:* 1615 Global Change: Biogeochemical processes (4805); 0315 Atmospheric Composition and Structure: Biosphere/atmosphere interactions; 3210 Mathematical Geophysics: Modeling; 0322 Atmospheric Composition and Structure: Constituent sources and sinks; 1610 Global Change: Atmosphere (0315, 0325); *KEYWORDS:* isotope model, ^{18}O in CO_2, isotope feedback mechanism, rectifier effect, global model

Citation: Cuntz, M., P. Ciais, G. Hoffmann, C. E. Allison, R. J. Francey, W. Knorr, P. P. Tans, J. W. C. White, and I. Levin, A comprehensive global three-dimensional model of $\delta^{18}O$ in atmospheric CO_2: 2. Mapping the atmospheric signal, *J. Geophys. Res.*, *108*(D17), 4528, doi:10.1029/2002JD003154, 2003.

[1]Laboratoire des Sciences du Climat et de l'Environnement, Unité Mixte de CNRS/CEA, Gif-sur-Yvette, France.
[2]Institut für Umweltphysik, Universität Heidelberg, Heidelberg, Germany.
[3]Division of Atmospheric Research, Commonwealth Scientific and Industrial Research Organisation, Melbourne, Victoria, Australia.
[4]Max-Planck-Institut für Biogeochemie, Jena, Germany.
[5]Climate Monitoring and Diagnostic Laboratory, NOAA, Boulder, Colorado, USA.
[6]Institute of Arctic and Alpine Research and Department of Geological Sciences, University of Colorado, Boulder, Colorado, USA.

Copyright 2003 by the American Geophysical Union.
0148-0227/03/2002JD003154

1. Introduction

[2] The emission of human induced CO_2, mostly in the northern hemisphere, causes the atmospheric CO_2 mixing ratio to increase with time and imprints a strong north-south gradient on the CO_2 mixing ratio. Regionally, Anthropogenic emissions of CO_2 are typically of the same order of magnitude as natural net CO_2 fluxes of the biosphere. This is different for the $\delta^{18}O$ isotopic composition of atmospheric CO_2. The fluxes for the isotopic CO_2 signal are called isofluxes and are a convolution of CO_2 fluxes and the difference between the isotopic ratio of these fluxes and the atmospheric isotope ratio. The latter difference is the apparent discrimination and the isoflux is the CO_2 flux multiplied by the apparent discrimination. This means that for the isotopic composition of atmospheric CO_2, the importance of each CO_2 flux can be attenuated or amplified by the apparent discrimination. *Peylin* [1999] showed that the global $\delta^{18}O$-CO_2 isoflux of anthropogenic emissions can be smaller by more than an order of magnitude in certain regions, compared to the global net (or total) $\delta^{18}O$-CO_2 isoflux of the biosphere. It is hence mainly the biosphere which defines the spatial distribution of $\delta^{18}O$-CO_2. (The gradient reflects in part the underlying gradient of the isotopic value of the soil water which is communicated, with modification, to the atmosphere only in the presence of fluxes with the terrestrial biosphere.) Because of the small seasonal variance of fossil fuel emissions, the seasonal cycle of $\delta^{18}O$-CO_2 is also mostly determined by the biospheric CO_2 gross fluxes, i.e., assimilation and respiration, which in contrast to fossil fuel combustion show big seasonal variations. To understand the atmospheric signal of $\delta^{18}O$-CO_2, it is therefore essential to understand the biospheric CO_2 fluxes and their associated apparent discriminations. On the other hand, one can learn about the biospheric CO_2 fluxes by examining the atmospheric $\delta^{18}O$-CO_2 signal.

[3] We have developed a comprehensive global three-dimensional (3-D) model of $\delta^{18}O$ in atmospheric CO_2, which is described in detail in a companion paper [*Cuntz et al.*, 2003] (hereinafter referred to as part 1). In the present paper, we focus on the modeled spatiotemporal distribution of atmospheric $\delta^{18}O$-CO_2. We examine the mean seasonal cycle of CO_2 and $\delta^{18}O$-CO_2 at atmospheric stations and the gradient of $\delta^{18}O$-CO_2 between the Arctic and Antarctica. Subsequently, we investigate the sensitivity of the model to different parameters, processes, and parameterizations.

2. Data and Model

2.1. Data Sets Used

[4] The GLOBALVIEW-CO_2 database presently consist of 165 stations at 118 locations with measurements of 22 different institutions [*GLOBALVIEW-CO_2*, 2002] (also available on Internet via anonymous FTP to ftp.cmdl.noaa.gov, Path: ccg/co2/GLOBALVIEW). The stations are distributed world-wide with a strong bias toward coastal or marine environments. Some stations are still influenced by close-by terrestrial sources and sinks but the majority select air measurements from the marine boundary layer (MBL) and are referred to as marine background stations. The stations that are considered to be MBL sites can be found in the GLOBALVIEW-CO_2 documentation. We added five non-MBL stations to GLOBALVIEW-CO_2 comprising four new aircraft sites in Eurasia [*Levin et al.*, 2002] plus one discrete sampling record at Schauinsland, Germany (SCH) [*Schmidt et al.*, 2001]. A characteristic of MBL stations is that discrete and (quasi-)continuous measurements are very close in the monthly or annual mean. Non-MBL stations show quite large deviations between means of continuous and discrete samples even if one applies filter methods to catch continental air representing large regions. Figure 1 shows the distribution of 59 stations that we used here for the comparison because we have $\delta^{18}O$-CO_2 data at these stations as well. Figure 2 presents seasonal cycles at 45 measurement sites (out of 59 stations in Figure 1) for which we have sufficient data to calculate seasonal cycles of $\delta^{18}O$-CO_2 (continuous measurements are open and discrete measurements are closed symbols; the lines are model results and are explained in the result section). We take the model values at the latitude, longitude and altitude of the stations as plain monthly means. We do not sample the model at different times to emulate special sampling strategies at individual stations but we shift sometimes the sampled latitude and/or longitude by one or two grid cells in order to take into account different sampling and filtering methods applied to the measurements [cf. *Ramonet and Monfray*, 1996]. One number after the station abbreviation represents the number of model grid cells or vertical layers by which we shifted the model. For example MHD1 means that we took one grid cell further to the west than the actual Mace Head coordinate to sample our model. The 4 aircraft sites have the designation '030' that is the GLOBALVIEW-CO_2 affix for aircraft measurements made at 3000 m height, e.g., SYK030 for aircraft measurements over Syktyvkar, Russia in 3000 m a.s.l. One can see the difference between MBL and non-MBL stations at, e.g., the two stations Point Barrow (BRW), MBL, and Schauinsland (SCH), non-MBL, where continuous and discrete sampling procedures are installed. Whereas Point Barrow shows almost no difference between continuous and discrete sampling, Schauinsland shows a peak-to-peak amplitude in the discrete record 1/3 of that in the continuous record. The continuous record at Schauinsland is filtered to exclude night-time values and low wind speeds [*Schmidt et al.*, 1996] whereas the flasks are filled during morning and may to some extent be influenced by local sources and sinks. Schauinsland is a mountain station situated 1205 m above the Rhine valley. We do not take the ground level on Schauinsland, in our model at about 360 m, but the fourth vertical layer at about 1300 m. Our model box is therefore far from local sources and sinks so that it is more comparable with the continuous measurements there. This is important to keep in mind when comparing $\delta^{18}O$-CO_2 monthly means of non-MBL flask records with model monthly means when the model was not sampled or filtered in the same way as the measurements.

[5] We merged further $\delta^{18}O$-CO_2 data at the 59 stations of Figure 1 where $\delta^{18}O$-CO_2 is measured on atmospheric flask samples. This includes 50 sites, named CMDL/INSTAAR, where the flasks were collected from the NOAA Carbon Cycle Group at the Climate Monitoring and Diagnostics Laboratory (CMDL) and measured afterward from the Stable Isotope Laboratory of the Institute for Artic and Alpine Research (INSTAAR) at the University of Colorado. At most stations, air was not dried in the NOAA Global Air Sampling Network before 1998/1999. *Trolier et al.* [1996]

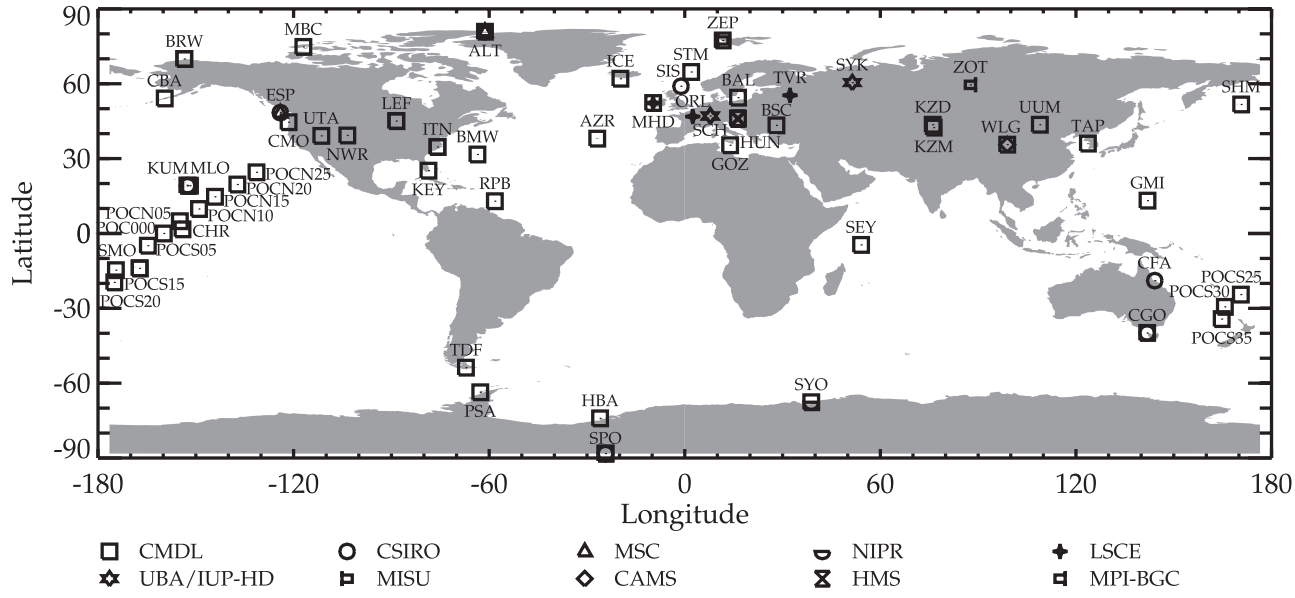

Figure 1. Global distribution of the 59 atmospheric measurement stations used in this study. Different symbols denote different laboratories that measure CO_2 (and δ^{18}O-CO_2).

found out that δ^{18}O-CO_2 measured at flasks collected at more humid sampling sites are most likely contaminated by exchange with water condensed on the flask wall [*Gemery et al.*, 1996]. CMDL/INSTAAR records from higher-latitude sites appear credible for δ^{18}O in atmospheric CO_2. Therefore we discarded all nondried flasks between 35°S and 35°N but kept the nondried flasks on all other latitudes.

[6] We added to the CMDL/INSTAAR stations seven stations with samples collected for and measured by the Division of Atmospheric Research at the Commonwealth Scientific and Industrial Research Organisation (CSIRO). The samples are all dried prior to filling so that the above problem does not apply to CSIRO data. CSIRO established a link to the VPDB-CO_2 scale in 1987 [*Francey and Goodman*, 1988]; however, with a change of mass spectrometer in 1991, the calibration of δ^{18}O-CO_2 was propagated under the assumption of similar instrument responses. A new assignment onto the VPDB-CO_2 calibration scale was introduced in 1999 (CG99) that recognized much greater susceptibility of the new mass spectrometer to "cross contamination" and thus removed a relative bias of around 0.8‰ in data obtained using the new mass spectrometer. Full details, including a minor revision of the CG99 assignment, are in preparation for publication. CMDL/INSTAAR and CSIRO measurements at the same stations differ now by this offset [*Masarie et al.*, 2001]. It is very likely that the CMDL/INSTAAR values are wrong by this offset because of erroneous standard material preparation. We shifted thus all CMDL/INSTAAR values by 0.8‰ to merge the two independent data sets. We focus in this paper on seasonal cycles and on the north-south gradient of δ^{18}O in atmospheric CO_2. The mean seasonal cycle in the merged data is not altered by the offset but the absolute annual mean values are, determining the north-south gradient change. However, both laboratories have a sampling site at South Pole, Antarctica, so that we can refer all annual means relative to the South Pole annual mean value of its sampling network and merge the respective north-south differences to give a consistent north-south gradient. Corrected for the 0.8‰ offset, the annual mean δ^{18}O-CO_2 at SPO was in 2000: 1.14‰ versus VPDB-CO_2 for CSIRO and 1.06‰ versus VPDB-CO_2 for CMDL/INSTAAR. Taking South Pole is somewhat arbitrary but South Pole station is far from sources and sinks of CO_2 and δ^{18}O-CO_2 and therefore reasonable as a reference point.

[7] As for CO_2, we added four δ^{18}O-CO_2 flask aircraft sites in Eurasia [*Levin et al.*, 2002] plus the δ^{18}O-CO_2 flask record at Schauinsland [*Schmidt et al.*, 2001]. Measurements of samples from these sites were made at the Institut für Umweltphysik, University of Heidelberg (IUP-HD), Laboratoire des Sciences du Climat et de l'Environnement (LSCE), Max-Planck Institut für Biogeochemie (MPI-BGC), and CSIRO. Because all five stations are non-MBL stations, they are only used here for comparison of the seasonal cycles so that systematic offsets between different labs [*Levin et al.*, 2003] play no role in this context. These stations were already used to analyze the East-West distribution of CO_2 and δ^{18}O-CO_2 over Eurasia [*Levin et al.*, 2002; *Cuntz et al.*, 2002] whereby systematic offsets may modify the statements made in these publications.

[8] The new combined data set of δ^{18}O-CO_2 shows slightly reduced seasonal amplitudes only at equatorial stations compared to a former data compilation [*Peylin et al.*, 1999] whereas it is rather similar over the rest of the globe. A north-south gradient of δ^{18}O-CO_2 of about 1.7‰ was recognized in the first six-site CSIRO data compilation in 1987 [*Francey and Tans*, 1987] and confirmed later by CMDL/INSTAAR measurements [*Ciais et al.*, 1997b; *Peylin et al.*, 1999]. The new combined data set exhibits an Arctic-to-Antarctic difference of 2.0‰ with very little interannual variability. We are confident that this is a robust feature of δ^{18}O-CO_2 and will not change in possible future data revisions.

2.2. Model Runs

[9] The model ECHAM/BETHY is described in detail in part 1. It is possible to run the model with or without the diverse processes described in part 1. The $CO^{18}O$ fluxes are calculated interactively with the δ^{18}O value of the atmo-

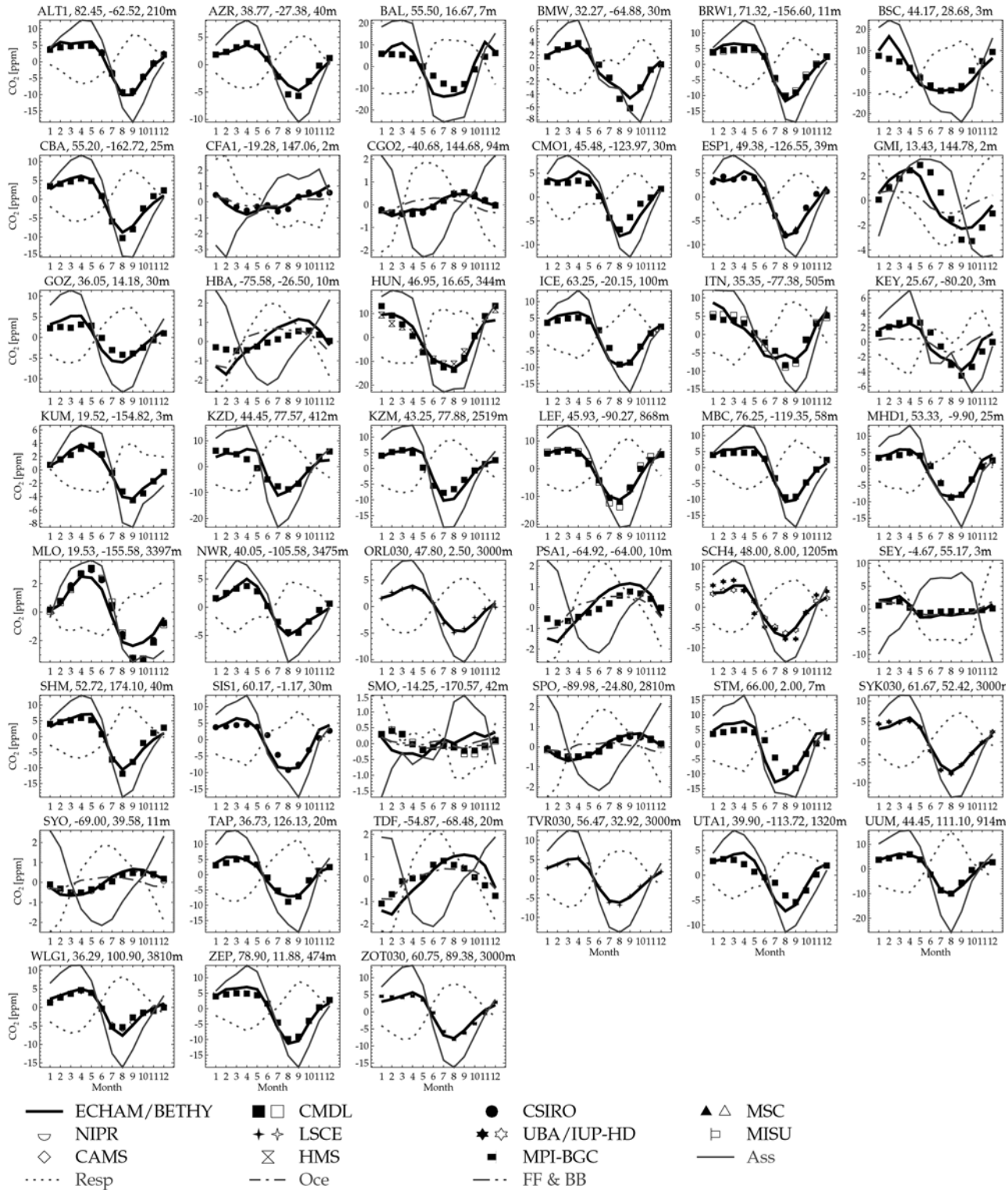

Figure 2. Mean seasonal cycle of CO_2 at atmosphere observatories. Measured monthly means are plotted with different symbols for each institution. Filled symbols are flask measurements of different laboratories, open symbols denote (quasi-) continuous measurements, the solid thick line is the ECHAM/BETHY standard run and thin lines show the contribution of each process. Individual processes are only plotted if their peak-to-peak amplitude exceeds 30% of the total model amplitude. Ass signifies assimilation (thin solid line), Resp respiration (thin dotted line), Oce the ocean contribution (thin dash dot line), and fossil fuel combustion and biomass burning are combined in FF & BB (thin dash triple dot line). Note that differences sometimes exist between laboratory CO_2 scales.

sphere, and therefore δ^{18}O will attain a different mean atmospheric level depending on the processes included in the particular model run. This can be seen from the global budget equation for δ^{18}O-CO_2 which we repeat here from part 1:

$$\frac{d\delta_a}{dt} = \frac{1}{C_a M_a}\left[F_R\Delta_R + F_A\Delta_A + F_{ao}\Delta_o^{des} + F_o\Delta_o^{equ} + \left(F_{fos} + F_{bur}\right)\Delta_f\right] \quad (1)$$

with

$$\Delta_R = \delta_s - \delta_a + \epsilon_s;$$

$$\Delta_A = -\epsilon_l + \frac{c_{cs}}{c_a - c_{cs}}(\delta_l - \delta_a);$$

$$\Delta_o^{equ} = \epsilon_w;$$

$$\Delta_o^{des} = \delta_o - \delta_a;$$

$$\Delta_f = \delta_f - \delta_a.$$

M_a is the conversion factor between fluxes in GtC and mixing ratios in ppm, Δ_A the discrimination of photosynthesis, Δ_o^{equ} the equilibrium discrimination between ocean and atmosphere. We explained in part 1 that we call the difference between the δ-value of the CO_2 flux and the atmospheric δ-value "apparent discrimination", for simplicity. Δ_R is thus the apparent discrimination associated to soil respired CO_2, Δ_o^{des} the ocean disequilibrium or the 'tendency' to equilibrate the difference between atmospheric and ocean dissolved CO_2, and Δ_f the difference between the isotopic signatures of O_2 and CO_2. The product of CO_2 flux and apparent discrimination is called isoflux. Writing the global budget equation in a short form gives:

$$\frac{d\delta_a}{dt} = k_1 - k_2\delta_a, \quad (2)$$

with

$$k_1 = \frac{1}{C_a M_a}\left[F_s(\delta_s + \epsilon_s) + F_A\left(\epsilon_l + \frac{c_{cs}}{c_a - c_{cs}}\delta_l\right) + F_{ao}\delta_o + F_o\epsilon_w + \left(F_{fos} + F_{bur}\right)\delta_f\right]$$

$$k_2 = \frac{1}{C_a M_a}\left[F_R + \frac{c_{cs}}{c_a - c_{cs}}F_A + F_{ao} + F_{fos} + F_{bur}\right]. \quad (3)$$

The solution of this differential equation is:

$$\delta_a(t) = \frac{k_1}{k_2} + \left(\delta_{a0} - \frac{k_1}{k_2}\right)\exp\{-k_2 t\}. \quad (4)$$

[10] So the global δ_a will stabilize at k_1/k_2 when t becomes much larger than k_2^{-1}. Including or excluding a process in a model run is like setting the appendant CO_2 flux to zero and k_1/k_2 will change accordingly. Table 1 repeats from part 1 the annual totals resp. annual mean values of ECHAM/BETHY variables.

[11] Our model stabilizes around a global δ^{18}O-CO_2 value of 2.3‰ versus VPDB-CO_2 including all processes and, e.g., around 3.0‰ versus VPDB-CO_2 taking only assimilation and respiration into account. The data, based on the CSIRO assignment onto the VPDB-CO_2 scale, indicate a global MBL surface mean of 0.5‰ versus VPDB-CO_2 (with a South Pole value of 1.1‰ versus VPDB-CO_2). In our model, the global mean value depends on what processes are included. For example, taking "invasion" into account (CO_2 isotopically equilibrated with soil water because of diffusion in and out of the soil, *Tans* [1998] and explained in detail in part 1), there is the extra term $F_{inv}\Delta_{inv}$ in the global budget equation (equation (1)) with $\Delta_{inv} = (\delta_s - \delta_a)$, the discrimination of invasion. This adds $F_{inv}\delta_s$ to the parenthesis of k_1 and F_{inv} to the parenthesis of k_2 (equations (2) and (3)). Our model calculates 18.6 GtC yr^{-1} CO_2 invasion flux that would reduce the global mean to 1.9‰ versus VPDB-CO_2.

Table 1. Global Annual CO_2 Fluxes, Assimilation Weighted Annual Mean CO_2 Mixing Ratios, Assimilation Weighted Annual Mean δ Values, and ϵ Constants Calculated and Used in ECHAM/BETHY[a]

Flux, Mixing Ratio, δ, ϵ	Value in ECHAM/BETHY
F_A	97.3
F_R	98.0
F_{ao}	99.4
F_o	2.6
F_{fos}	5.8
F_{bur}	3.1
c_a	353
c_{cs}	264
δ_l	6.3
δ_s	−6.9
δ_o	1.2
δ_f	−17.0
ϵ_l	−7.4
ϵ_s	−7.2
ϵ_w	0.8

[a]Global annual CO_2 fluxes are given in GtC yr^{-1}, assimilation weighted annual mean CO_2 mixing ratios are given in ppm, assimilation weighted annual mean δ values are given in ‰ versus VPDB-CO_2, and ϵ constants are given in ‰.

[12] When we start the model from one particular global uniform value, δ_{a0}, in the atmosphere, k_2^{-1} denotes the e-folding time of the stabilization. The e-folding differs between 1.3 and 1.9 years depending on the processes included and it needs at least 3 e-folding times to establish a stable annual mean north-south gradient. So we initialize our model with 0‰ versus VPDB-CO_2 everywhere and let the model run for 15 years. We then take the mean of the last 5 years for our analyses. The model is not sensitive to δ_{a0} but the stabilization process is always determined by k_2. Our sub-daily time step produces rather a seasonally cyclo-stationary result than a fixed asymptote, i.e., that the model shows seasonal variations around an asymptote, which is exactly k_1/k_2. An exponential fit to the global model δ^{18}O-CO_2 value during spin-up gives also exactly k_2^{-1} as e-folding time. Our standard model run includes the same processes as included by *Ciais et al.* [1997a, 1997b], namely assimilation, respiration, ocean exchange, fossil fuel combustion, and biomass burning. Individual process contributions to the atmospheric δ^{18}O-CO_2 signal are not just the δ-values, which would occur if only the individual process were present, δ^i, because δ is not a conserved quantity. $c^i\delta^i$ in contrast is a mass conserving tracer with c^i as the contribution of process i to the overall CO_2 mixing ratio. The contribution of an individual process

is thus calculated as the normalized $c^i\delta^i$ relative to an atmospheric background value, δ^{bg}, and is called δ-anomaly, δ^i* [*Heimann and Keeling*, 1989]:

$$\delta^{i*} = \frac{c^i\left(\delta^i - \delta^{bg}\right)}{\sum_i c^i} = \frac{c^i\left(\delta^i - \delta^{bg}\right)}{c_a}. \quad (5)$$

δ^{bg} is taken as 0‰ versus VPDB-CO_2. The sum of all δ^i* gives $\delta_a - \delta^{bg}$. They are hence additive whereas the individual δ^i are not (compare, e.g., the results of *Peylin et al.* [1997], who used δ^i*, with the results of *Ciais et al.* [1997b], who used δ^i).

3. Results and Discussions

[13] The δ^{18}O value of atmospheric CO_2 depends on the CO_2 fluxes and the apparent discriminations of the involved processes. It is therefore essential to model properly atmospheric CO_2 values. We showed in part 1 that ECHAM/BETHY computes generally very realistic CO_2 fluxes. These are transported in ECHAM and the resulting signal is compared here to atmospheric observations. We focus then on the comparison between measured and modeled atmospheric δ^{18}O-CO_2.

3.1. CO_2 Seasonal Cycle

[14] We show in Figure 2 mean seasonal cycles of atmospheric CO_2 at the 45 selected stations, alphabetically sorted by their GLOBALVIEW-CO_2 abbreviation. The seasonal cycle is mostly determined by assimilation and respiration so that another process becomes important only at 11 out of 45 stations. ECHAM/BETHY performs very well at most stations with 10 evident exceptions, namely Baltic Sea (BAL), Black Sea (BSC), Mariana Islands, Guam (GMI), Halley Station, Antarctica (HBA), Mauna Loa, Hawaii (MLO), Palmer Station, Antarctica (PSA), Tutuila, American Samoa (SMO), Norway Shipboard (STM), Tierra Del Fuego, Argentina (TDF), and Wendover, Utah (UTA). The Baltic is a closed basin in the ECHAM T21 spectral truncation. Therefore the nearby continental signal is transported very quickly over the basin so that BAL is influenced excessively by adjacent terrestrial biosphere fluxes in the model. The Black Sea does not exists at all in the T21 truncation. However, BSC station is located at the west coast of the Black Sea so that BSC in the model will "see" a totally different micro-climate than the measurement station BSC. Tutuila (SMO) lies in the Pacific Ocean. The South Pacific Convergence Zone (SPCZ) passes over SMO only once per year in the model so that it misses the peculiar form of the seasonal cycle at SMO. A similar problem in simulating the passage of the Intertropical Convergence Zone (ITCZ) is present in ECHAM T21 truncation at Christmas Island (CHR, not shown here). This is likely a resolution-dependent problem with T21 being too coarse. However, it seems that the problem of ECHAM T21 exists only in the Pacific Ocean because ECHAM/BETHY captures the peculiar seasonal cycle of Mahe Island, Seychelles (SEY) in the Indian Ocean and at Ascension Island in the Atlantic Ocean (not shown here because we have no δ^{18}O-CO_2 measurements there), the seasonal cycles of both are also mainly determined by the ITCZ. The modeled amplitude is too low at Mariana Islands (GMI) and too high at Wendover (UTA) and both show a phase shift of about one month compared to the data. We showed in part 1 that it is possible that this behavior comes from a incorrect timing between assimilation and respiration. Shifting the respiration CO_2 contribution in the output of the model does indeed lead to a much better agreement between model and measurements at GMI and UTA. Halley Station (HBA), Palmer Station (PSA), and Tierra Del Fuego (TDF) lie all around the Antarctic circumpolar current and are strongly influenced by the ocean CO_2 net flux. ECHAM4 has up to 6 m s^{-1} stronger winds in the southern ocean during summer compared to reanalyses of the European Centre of Medium-range Weather Forecast (ECMWF) [*Roeckner et al.*, 1996] which results in a higher CO_2 ocean sink in the vicinity of Antarctica (oceanic CO_2 fluxes are parameterized with speed, see part 1). Comparing Cape Grim (CGO) and South Pole (SPO) with stations at the intervening latitudes (HBA, PSA, TDF) shows that the peak-to-peak amplitude of the mean seasonal cycle in the model is very similar at CGO and SPO but doubled in between. This suggests an ocean effect at the Antarctic coastal stations. Mauna Loa (MLO) and Cape Kumukahi (KUM) are two stations on Hawaii. MLO station is situated in 3397 m on the northern flank of the Mauna Loa volcano. KUM is a ground station on the eastern most projection of the island of Hawaii. The peak-to-peak amplitude at MLO is only about 60% of the KUM amplitude and its phase lags by about one month. ECHAM/BETHY catches well the seasonal cycle at KUM but is too weak at MLO. It is recognized that the vertical advection in ECHAM is too strong for tracers [*Timmreck et al.*, 1999] but that convection is quite realistically reproduced [*Mahowald et al.*, 1995]. So it depends on the relative strength of vertical advection and convection around sources to simulate high-altitude stations well and these could be poorly represented by ECHAM/BETHY. This could be the reason why the Norwegian Shipboard (STM) station is out of phase by one month with excess amplitude. We showed in part 1 that the maximum in Net Ecosystem Exchange (NEE) occurs in June/July in Europe but most northern hemispheric atmospheric stations show their minimum in atmospheric CO_2 in August/September. This time-lag comes from the atmospheric transport which accounts for about one month [*Ciais et al.*, 2001]. The model, however, shows an immediate response to NEE fluxes in atmospheric CO_2 at STM with an even earlier July minimum in the atmosphere.

3.2. The δ^{18}O-CO_2 Seasonal Cycle

[15] ECHAM/BETHY provides good simulations of the seasonal cycle of CO_2 at most stations. The seasonal cycle of δ^{18}O in atmospheric CO_2 at the same 45 stations is shown in Figure 3. As for CO_2, we plot all processes with amplitude at least 30% of the total model amplitude. The seasonal cycle in δ^{18}O-CO_2 is almost completely determined by assimilation and respiration. There are only two stations where another process has a noticeable influence. There is an oceanic influence at Halley Station, Antarctica (HBA) and a contribution of fossil fuel combustion at Mahe Island, Seychelles (SEY). SEY receives northern hemispheric air during northern spring, summer, and autumn

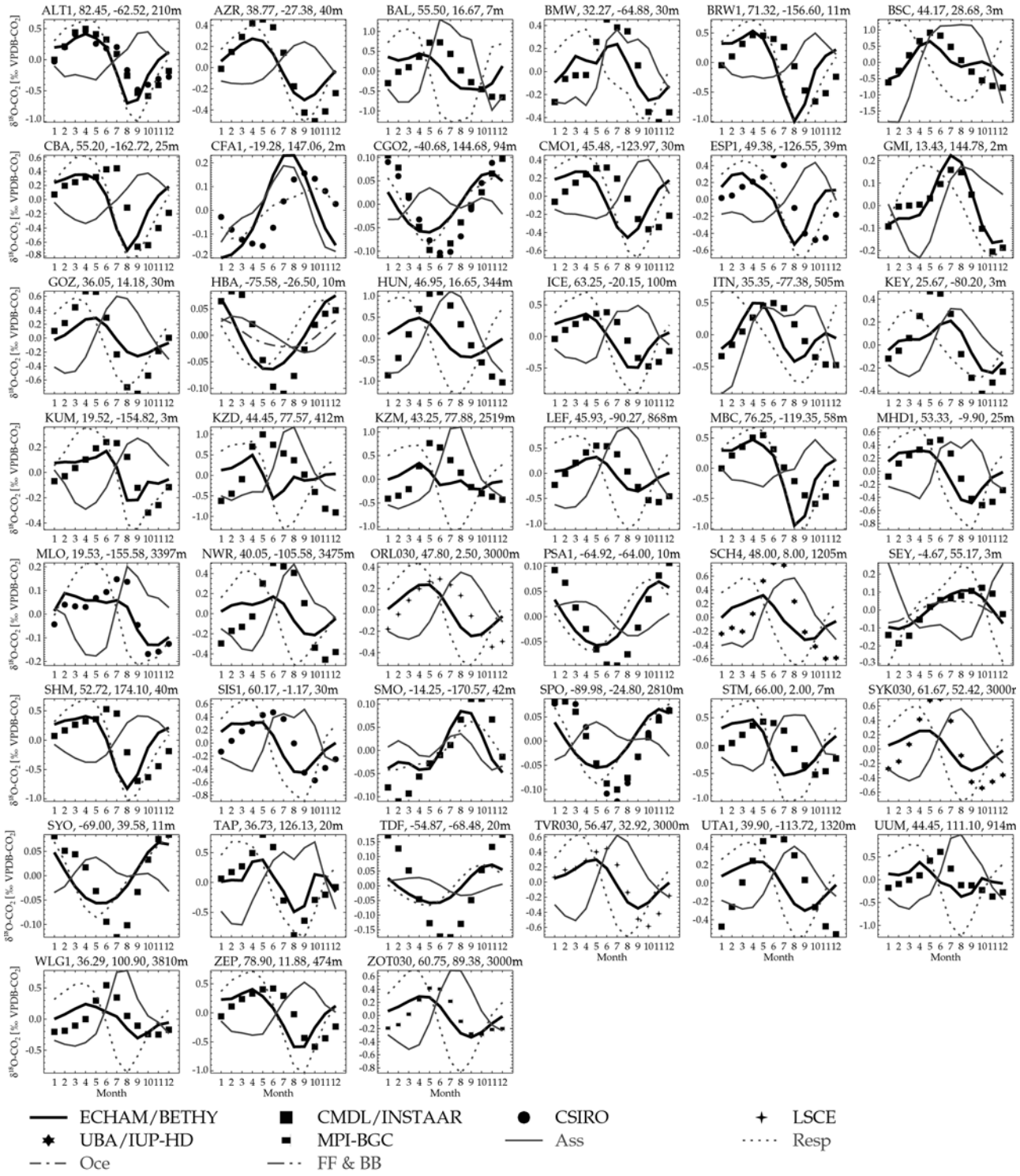

Figure 3. Mean seasonal cycle of δ^{18}O-CO_2 at atmosphere observatories. Symbol and line definitions are the same as in Figure 2. Note that differences sometimes exist between laboratory δ^{18}O-CO_2 scales.

and southern hemispheric air during winter. This leads to a different contribution of fossil fuel combustion in winter against the rest of the year and leads to a transport contribution at SEY. Our model shows the correct amplitude at high northern hemispheric stations but with a two months phase shift, e.g., at Alert (ALT), Barrow (BRW), or Mace Head (MHD). There δ^{18}O-CO_2 has its minimum in October whereas our model shows its minimum in August as for CO_2. This time lag is present at almost all stations. It was also present in earlier δ^{18}O-CO_2 models [e.g., *Peylin et al.*, 1999], not as pronounced in the high northern and southern latitudes but with the same strength elsewhere. The model fails to catch the amplitude of the seasonal cycle outside the high northern latitudes where it calculates about 2/3 of the measured amplitude. Peylin et al. concluded that respiration is the dominant process controlling the seasonal cycle and

that assimilation acts like a correction to the respiration dominated seasonal cycle. As explained in part 1, we calculate CO_2 fluxes and isofluxes directly in our model so the apparent discriminations are the ratio of isoflux to CO_2 flux. Our leaf discrimination is therefore assimilation weighted on a sub-daily basis, making it bigger and strengthening its influence. Assimilation has the same influence on δ^{18}O-CO_2 as respiration in our model in contrast to offline models like those of *Ciais et al.* [1997a, 1997b] and *Peylin et al.* [1997, 1999], so that the assimilation processes parameterizations become more important in our model. For example, as explained in part 1, changing only the non-water-limited stomatal CO_2 mixing ratio, c_{i0}, within the range of parameter sets found in the literature, does not significantly change assimilation but alters the amplitude of δ^{18}O-CO_2 at high northern hemispheric stations by a factor of 2 due to the factor $c_{cs}/(c_a - c_{cs})$ in leaf discrimination (see equation (1)). We have chosen the higher c_{i0} because they are derived from a literature survey of field measurements (*Schulze et al.* [1994] and part 1) rather than from laboratory measurements (*Farquhar et al.* [1989], *Boyer et al.* [1997], and part 1). However, other parameter choices may equally be suitable or justifiable. The c_{i0} values are most important at high northern latitudes where water-limitation is less prevalent and plants are limited by factors other than water. Note that southern hemisphere stations outside the tropics show generally very small seasonal cycles, reduced by a factor of 10 compared to northern hemispheric stations (compare South Pole (SPO) with a peak-to-peak amplitude of 0.15‰ to Alert (ALT) with an amplitude of approximately 1‰). They are therefore hard to measure and one can see at SPO differences in the data between CMDL/INSTAAR and CSIRO. Anyway, our model shows only 2/3 of the amplitude outside high latitudes but it is without doubt possible to find a reasonable parameter set which fits the amplitude at the stations. For the time being, we persist with the parameters of Ciais et al. and Peylin et al. for comparison but fixed a value of $\epsilon_s = -7.2$‰ [*Miller et al.*, 1999] which was a fit parameter in earlier models in order to have no atmospheric trend.

[16] There are a number of phenomena in the CO_2 and δ^{18}O-CO_2 data which are of interest:

[17] 1. One expects a time lag between the phasing of the production function (CO_2 fluxes and isofluxes) and the phasing of the seasonal cycle of the atmospheric concentrations because (1) the atmosphere integrates over recent production and (2) the trace gases have to be transported from the site of production to the stations. Northern hemispheric NEE measurements, shown in part 1, exhibit their minimum NEE in June/July and northern hemispheric CO_2 measurements in the atmosphere show their minimum in August/September (e.g., BRW, ICE, SIS, SYK, and ZOT). So there is a 1–2 month time lag between NEE and the atmospheric CO_2 measurements. The transport can be separated into horizontal and vertical transport and one can state that mostly vertical diffusion is responsible for the time lag in concentrations between the surface and high altitudes. ECHAM/BETHY reproduces the observed seasonal cycle of CO_2 very well, at ground stations as well as at altitude stations. The source function of δ^{18}O-CO_2 has the same timing then NEE in our model so that CO_2 and δ^{18}O-CO_2 show their minimum at the same time in the model, at ground as well as at altitude stations. However, the δ^{18}O-CO_2 observations show a time lag of two month between CO_2 and δ^{18}O-CO_2 that is not captured by ECHAM/BETHY.

[18] 2. A well known example of the difference between ground and altitude stations is the station pair Kumukahi (KUM) and Mauna Loa (MLO), both situated on Hawaii, KUM at ground and MLO more than 3 km above sea level. MLO exhibits therefore a one month time lag in the CO_2 seasonal cycle compared to KUM. It is interesting to recognize that MLO and KUM show their minimum in CO_2 and δ^{18}O-CO_2 at the same time in the observations whereas ECHAM/BETHY reproduces the time lag for CO_2 at MLO for δ^{18}O-CO_2 as well.

[19] 3. At some continental stations, δ^{18}O-CO_2 lags even further behind CO_2: e.g., 3 months at SCH, 4 months at BSC, and 5 months at KZM. ECHAM/BETHY does not reproduce these features but is very uniform in its response at the atmospheric stations, i.e., it shows the δ^{18}O-CO_2 minimum the same time as CO_2 at ground stations and 1 month lagged at high-altitude stations.

[20] 4. δ^{18}O-CO_2 in the southern hemisphere shows very small seasonal cycles with peak-to-peak amplitudes of about 0.2‰. A 'good' pair-to-pair difference between flasks filled simultaneously is about 0.05‰. If flasks are stored for a long time (e.g., at South Pole), CO_2 has time to exchange isotopically with residual water. However, this depends on the origin of tracer-water in the flasks and the temperatures during storage and transport. δ^{18}O-CO_2 in the southern extratropics is very similar at all stations (CGO, HBA, PSA, SPO, and SYO) and we have been able to locate systematic measurement or data treatment biases that would contribute a significant seasonal artefact. In the southern hemisphere, the measurements and ECHAM/BETHY predictions are thus both uniform; the model precedes the data by one to two months, and shows only 2/3 of the measured amplitude.

[21] We examine the seasonal cycle of ECHAM/BETHY further in section 3.4 where we explore the behavior of ECHAM/BETHY due to modified parameters, changed parameterizations, and the inclusion or exclusion of different processes.

3.3. North-South Gradient and Rectifier Effect

3.3.1. Imbalance of Isofluxes in Latitude

[22] By construction, the biospheric fluxes are equilibrated, i.e., we have locally no annual mean net CO_2 flux to or from the biosphere. However, the corresponding δ^{18}O gross fluxes, or isofluxes, being the convolution of CO_2 fluxes and apparent discriminations, may not be equilibrated. Indeed, if the annual mean leaf discrimination does not equal the apparent soil discrimination, the total biospheric isoflux can be nonzero. Consequently, in our coupled model, the atmospheric δ value will change according to equation (1). Since δ_a feedbacks on leaf and apparent soil discrimination, its global value will finally stabilize at k_1/k_2 (see equations (1)–(3)) and the annual mean leaf and apparent soil discriminations will adjust to cancel each other. Making a run with only biospheric fluxes, δ_a stabilizes at about 3‰ versus VPDB-CO_2 with isofluxes of + and −1650 GtC ‰ yr^{-1}, for assimilation and respiration respectively, which is equivalent to global apparent discriminations of about ±16.8‰. However, leaf and soil isofluxes are not equal in every grid

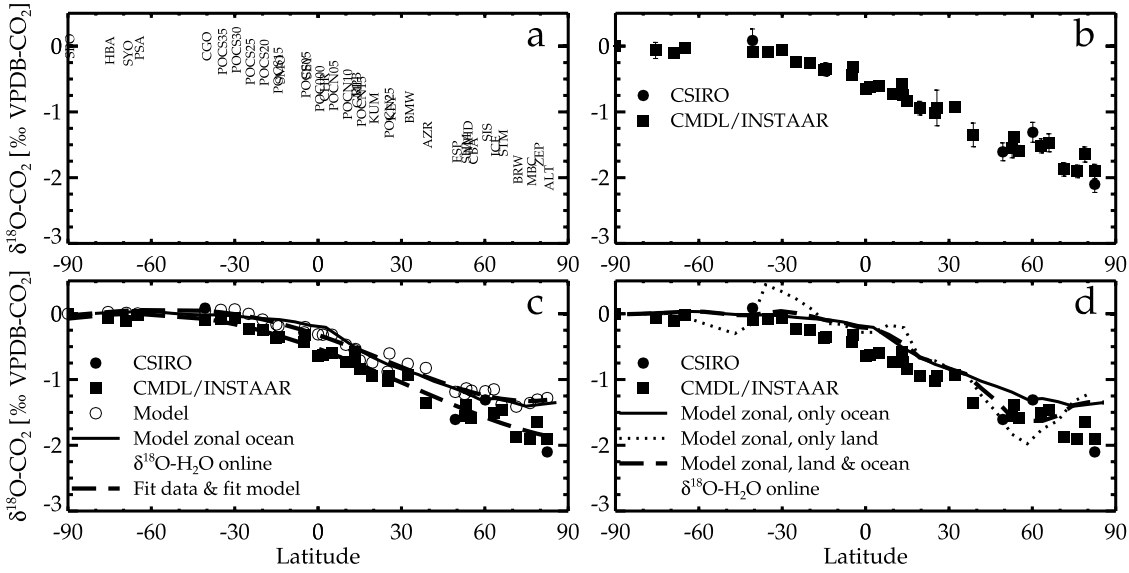

Figure 4. Meridional gradient of δ^{18}O-CO_2 relative to South Pole. For simplicity, Figure 4a shows each MBL station's abbreviation centered over its mean value relative to South Pole; if both laboratories collect measurements at a particular station, the station's abbreviation is centered over the mean of both laboratories. Figure 4b shows the same data, but symbolized for each individual laboratory with errorbars signifying the standard deviation of inter-annual variations at the station relative to South Pole. In Figure 4c, the data are as in Figure 4b, but with ECHAM/BETHY results at the station coordinates as open circles together with least squares fits of 4 polynomials through data and through model values (dashed lines) as well as the latitudinal mean of the lowest model layer of ocean grid cells (solid line), Figure 4d the same symbols as in Figure 4c, but with the latitudinal mean of ocean grid cells (solid line), land grid cells (dotted line) and all grid cells (dashed line).

cell unlike for CO_2 assimilation and respiration fluxes (see part 1) because equation (1) is only valid for the globe, but in one atmospheric grid box, there is also transport from adjacent grid boxes that change the atmospheric δ^{18}O-CO_2. Leaf isoflux is about the same in the northern and southern hemispheres, adding up to 825 GtC ‰ yr^{-1} per hemisphere in the biosphere-only run. This is because northern hemispheric net assimilation accounts for 57.3 GtC yr^{-1} and southern hemispheric net assimilation for 40.0 GtC yr^{-1} leading to leaf discrimination of 14.4‰ and 20.6‰, respectively in both hemispheres. In contrast, soil isoflux does not apportion equally between the two hemispheres: −985 GtC ‰ yr^{-1} in the northern hemisphere and −665 GtC ‰ yr^{-1} in the southern hemisphere, yielding apparent soil discriminations of −17.1‰ and −16.4‰, respectively. There is therefore an imbalance in the isofluxes between northern and southern hemisphere. The southern hemisphere emits an isoflux of +160 GtC ‰ yr^{-1} which is balanced in the northern hemisphere by a total isoflux of −160 GtC ‰ yr^{-1}. This is mirrored, through atmospheric transport, in a north-south gradient in the atmospheric δ^{18}O-CO_2 values.

3.3.2. Modeled and Observed Latitudinal Gradient in δ^{18}O-CO_2

[23] We show in Figure 4 the north-south gradient of δ^{18}O-CO_2. We added to the 45 stations of the seasonal cycle analysis 11 ship ''stations'' between 35°S and 35°N (POCS35 to POCN35), Christmas Island (CHR), Ragged Point, Barbados (RPB), and Gobabeb, Namibia (NMB) where either the record length or the data density were not sufficient to calculate a seasonal cycle; but the absolute atmospheric level should not be corrupted. Only CSIRO and CMDL/INSTAAR data were considered. We then excluded all non-MBL stations, which are under more regional continental influences, including rectification effects (see below). We included in Figure 4c ECHAM/BETHY predictions at the actual stations together with the zonal mean of the lowest model layer over ocean grid cells, which we consider as being more closely comparable to the data. To demonstrate this, we did two least squares fits of a polynomial function, one to the measurements and one to the model values at the stations. The χ^2 of the least squares fits does not change significantly if we used more than 4 polynomials. One can see for the model values that the fit deviates only in the tropics from the latitudinal mean of ocean grid cells and is otherwise nearly identical to it. A cubic fit, often used to represent measurements of CO_2 [e.g., *Denning et al.*, 1995], had much higher χ^2 values and did not represent the measurements as accurately. We can compare in Figure 4d the latitudinal means of all grid cells, of only ocean grid cells, and of land grid cells only. The conventionally used latitudinal mean of all grid cells to represent the north-south gradient is very similar for δ^{18}O-CO_2 to the only ocean only latitudinal mean but shows a local minimum at around 60°N. This is the combined effect of continental isofluxes and of their covariance with atmospheric transport patterns, which is analyzed next.

3.3.3. Covariance Between CO_2 Biospheric Fluxes and Atmospheric Transport

[24] In the case of CO_2, even with locally, annually balanced fluxes, covariance between horizontal and vertical

transport and the diurnal, seasonal fluctuations in NEE generates annual mean CO_2 gradients, which are referred to generically as rectification gradients. In our model that includes diurnal and seasonal variations in NEE, rectification gradients show off as a north minus south difference of 2.5 ppm (Figure 5) which is even bigger than the estimate of *Denning et al.* [1995]. Taking a plain latitudinal mean over all grid points shows two broad maxima, one around the equator, and one around 55°–60°N, reaching values of 5 ppm (Figure 5). The same behavior can be seen in the TRANSCOM project phase 1 [*Law et al.*, 1996] where models with a high rectifier effect show all maxima around 60°N and a drop in mixing ratio afterward. Such latitudinal signal is not sampled in the actual station network of GLOBALVIEW-CO_2, where most of the sites are MBL stations, and we thus decided to use only ocean grid points to safely compare measurements with model latitudinal means. *Tans et al.* [1990] and *Denning et al.* [1995] bypassed this problem by using a fit through modeled station values. Figure 4c shows that both approaches are very similar whereas considering the latitudinal mean over ocean grid cells is easier to calculate, more robust to the fit procedure used, and less sensitive to a wrong station representation in the model (e.g., data selection, smoothed model orography, etc.) [cf. *Ramonet and Monfray*, 1996].

[25] We show in Figure 6 the spatial distribution of CO_2 related to the biospheric fluxes. We subtracted from all atmospheric values the trend at South Pole as a reference to make Figure 6 directly comparable with Figures 4 and 5. Vertical transport during daytime in the growing season is vigorous when the Net Ecosystem Exchange (NEE) is negative, giving a sink. This results into only a small negative gradient in CO_2 mixing ratio between the surface and the Planetary Boundary Layer (PBL). Vertical transport is almost suppressed during nighttime when NEE is positive, giving a source. This yields a strong positive gradient in mixing ratio between the surface and the PBL. Taking the daily (monthly) mean in one height leads to a shift in CO_2 mixing ratio that is positive near the ground and negative in the higher PBL, i.e., the average values are higher at the ground than in mid-PBL. The magnitude of the vertical gradient due to diurnal flux-transport covariance, sometimes called Diurnal Rectifier Effect, obviously varies throughout the season [*Stephens et al.*, 1999], as can be seen in tall tower CO_2 measurements [e.g., *Bakwin et al.*, 1998]. Beyond daily timescales, transport patterns in summer and winter are on average different, e.g., higher wind speeds inside the continents during winter lead to a faster dilution of concentration differences, and they covary as well with the seasonal pattern of negative NEE during summer and positive NEE during autumn/winter [*Ciais et al.*, 2000; *Taylor*, 1998]. This seasonal covariance controlling the spatial patterns of CO_2 shows up in models even without diurnal cycles, and it is often called Seasonal Rectifier Effect. Both rectifier effects are superimposed in nature and in our model, whereby the diurnal rectifier effect contributes about 80% of the amplitude over land and only 25% of the amplitude over ocean [*Denning et al.*, 1996b]. In Figure 6g over the ocean, one can hardly detect the CO_2 interhemispheric gradient of Figure 5 because it is lower than the steps of the color scale but one can easily spot the local maximum of CO_2 in the northern boreal zone which

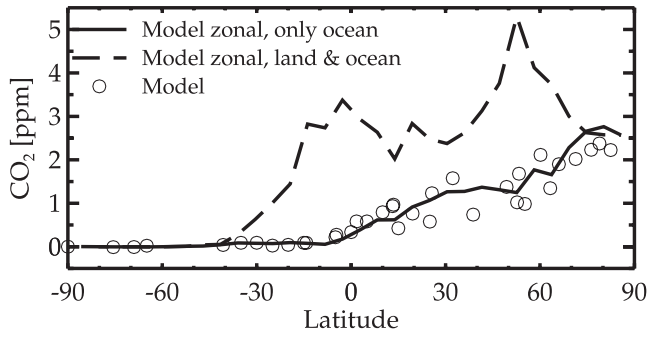

Figure 5. Meridional gradient of CO_2 relative to South Pole in ECHAM/BETHY for a biosphere-only run (biosphere in equilibrium). Open circles are the model sampled at the individual stations, the solid line is the latitudinal mean of atmospheric CO_2 over ocean grid cells in the lowest model layer, and the dashed line is the latitudinal mean of all grid cells in the lowest model layer (land and ocean).

leads to the characteristic maximum at 60°N in Figure 5, and is entirely implied by rectification processes. The third model level lies in the middle of the PBL (approximately 800 m) in summer but outside of the PBL in winter and during night (most times). ECHAM/BETHY shows a very strong accumulation of CO_2 at the ground level with respect to the third level (third column in Figures 6a–6i) over the continents most of the time. The difference between ground and mid-PBL gets negative only in eastern Siberia and in Alaska in July (Figure 6f). The very low daily amplitude of NEE in those two Arctic regions covaries there with a zonal transport which is stronger than the vertical transport, i.e., that the seasonal rectification processes outweighs diurnal rectification processes in those regions. The Amazon and Equatorial Africa regions show generally the biggest CO_2 rectification gradients yielding accumulations near the ground of up to 20 ppm in the annual mean compared to surrounding ocean grid boxes (Figure 6i). Daytime convection is very strong and repetitive over the Amazon and together with high NEE amplitudes [*Araújo et al.*, 2002], this leads to a strong diurnal rectifier signal. For the same reasons, East-Europe, West-Siberia, and South-East-Asia show as well very large vertical rectification gradients between ground and 800 m in July which attain values of up to 30 ppm (Figure 6f) comparable with rectification gradients in the Amazon (Figure 6c). It is nevertheless surprising that the average ground level CO_2 over Eurasia shows lower values than over the ocean almost everywhere in July (Figure 6d). The rectification effects get revealed there only in the difference to the 800 m level (Figure 6f).

3.3.4. Covariance Between δ^{18}O-CO_2 Biospheric Fluxes and Atmospheric Transport

[26] In the case of δ^{18}O, we also expect rectification effects to be strong, as for CO_2 discussed above. In addition, since the δ^{18}O-CO_2 budget is not closed on every grid cell, rectification gradients are everywhere convoluted with gradients induced by nonzero annual mean isofluxes. We show in Figure 6 the spatial distribution of δ^{18}O in CO_2 related to biospheric fluxes. Conceptually, the picture is similar to the one of CO_2, with accumulation over the continents and a more uniform meridional distribution over the oceans.

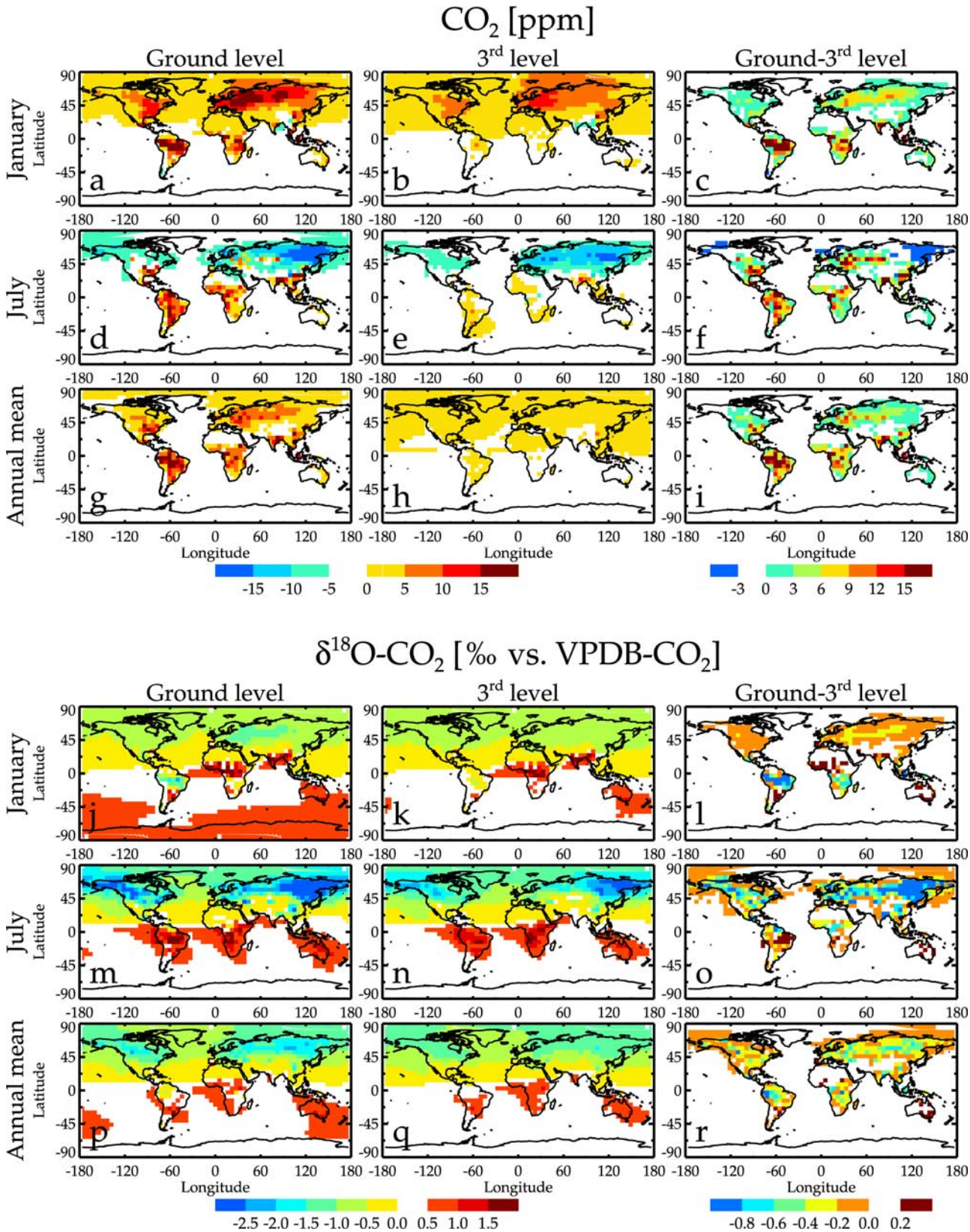

Figure 6. (a–r) Rectifier effect of the biospheric fluxes in ECHAM/BETHY for CO_2 and δ^{18}O-CO_2. The first column is the ground level (around 30 m), the second column the third model level (around 800 m), and the third column is the difference between ground and third level. Note that the color bar in the third column differs from the combined color bar for column one and two. We subtracted the trend at South Pole from each grid point as a reference.

Accumulations of CO_2 near the ground over active vegetation are generally mirrored by more negative δ^{18}O-CO_2 values. An exception to this is the Amazon where the isotopic enrichment effect of leaves dominates almost all year-round the isotopic depletion induced by respiration. However, the ground minus mid-PBL vertical difference in δ^{18}O is still negative over the Amazon (Figure 6r), because the negative isoflux signal of respiration accumulates in shallow nocturnal boundary layers. The negative difference of CO_2 between ground and mid-PBL over Eastern Siberia and Alaska in July (Figures 6d–6f) is mirrored by very negative differences in δ^{18}O-CO_2 (Figures 6m–6o). This comes from negative leaf discrimination in this region in the model, which superimpose on rectification effects similar to those of CO_2 (see part 1 and *Cuntz et al.* [2002]). This affects the annual mean vertical distribution of δ^{18}O-CO_2 in such a way that, overall, δ^{18}O-CO_2 at the ground is more negative than at 800 m over the whole Eurasian and the North-American continents (Figure 6r) whereas CO_2 shows an accumulation over land only in Eastern Europe, Western Siberia, and over the North American East Coast (Figure 6i). One can see over the ocean the north-south gradient of Figure 4 in Figure 6p, with values about −2.0‰ versus VPDB-CO_2 lower than at South Pole between 45°N and 60°N. Over land however, in the same mid-northern latitude band, δ^{18}O-CO_2 is reduced to −2.5‰. This is the minimum in the δ^{18}O-CO_2 north-south gradient of all grid points in Figure 4d and present in earlier δ^{18}O-CO_2 modeling studies [*Ciais et al.*, 1997b; *Peylin et al.*, 1999].

[27] In summary, both δ^{18}O and CO_2 are subject to the same rectification processes, affecting the annual mean spatial distribution of both species, in particular their ocean-land contrast near the ground. Rectification processes are present in the world of models and likely in the real world as well, superimposed with the signal of mean sources and sinks. Uncertainties in modeled rectifications translate therefore in huge errors when applying inverse modeling techniques to the present set of stations. Noting the importance of gross fluxes for δ^{18}O-CO_2 and of net fluxes for CO_2, the small imbalance of CO_2 sources and sinks plays a role essentially for CO_2 but very minor for δ^{18}O-CO_2. Therefore (with optimism), if we knew the isofluxes very well, including their diurnal and seasonal patterns (for instance from systematic studies at eddy covariance towers [e.g., *Bowling et al.*, 1998]), then δ^{18}O-CO_2 could be used in the future to validate independently from CO_2 rectification effects in atmospheric transport models.

3.4. Sensitivity Studies

[28] Our standard run includes assimilation, respiration, ocean fluxes, fossil fuel combustion and biomass burning. These are the same processes that *Ciais et al.* [1997a, 1997b] included in their model study. First, they claim that assimilation and respiration are responsible for the seasonal cycle of δ^{18}O-CO_2 but that one needs fossil fuel combustion input and the biomass burning process to simulate a realistic north-south gradient. We performed several sensitivity runs that are summarized in this section, notably we included or excluded a variety of processes, and added new processes that were explained in part 1. Specifically, we changed further the globally fixed fractionations, and changed the formulation of some processes. We show in the plots only a selection of these sensitivity runs because δ^{18}O-CO_2 in ECHAM/BETHY is almost exclusively determined by assimilation and respiration.

[29] We label in Table 2 only the sensitivity studies which are discussed in the text in detail and show which processes are included in the runs. For example, AR stands then for the run which includes only assimilation and respiration and STD denotes our standard run. We added in the sensitivity runs each time one process extra to the AR run to examine the influence of each process individually. For example, we added ocean CO_2 exchange fluxes to the AR run, named AROCE. ARMM denotes a model run where the online calculated water isotopic composition was replaced by monthly mean input fields of δ^{18}O-H_2O of rain and vapor. STD is our standard run including the processes of *Ciais et al.* [1997a, 1997b] and the water isotopic composition is calculated online at each time step in the model. STDMM replaces therein the online calculated water isotopes again with monthly means of δ^{18}O-H_2O of rain and vapor.

3.4.1. Sensitivity of δ^{18}O-CO_2 North-South Gradient

3.4.1.1. Feedback of δ_a

[30] Previous models of δ^{18}O in atmospheric CO_2 described the influence of different processes on the north-south gradient as well. We show in Figure 7a the contribution of each individual process to the latitudinal mean of δ^{18}O-CO_2 of the standard run. Respiration and assimilation show by far the strongest influence on the total signal, making each about −0.6 to −0.7‰ of the total signal of approximately −1.5‰. The oceanic and burning contributions are small, contributing only slightly less than +0.1 and −0.2‰ respectively to the overall north-south gradient. The Figure seems to suggests that if one removes one process, the total signal is also reduced by this process. However, this is not true in the online model because adding or removing a process feedbacks on the global δ^{18}O-CO_2 level in the atmosphere, therefore changes apparent discriminations and thus the contributions of all other processes to the atmospheric signal. This can be studied in Figures 7b and 8, where we plotted the results of several sensitivity runs. For example, adding up assimilation and respiration in Figure 7a gives a δ^{18}O-CO_2 value at the North Pole of −1.2‰ (relative to South Pole). The total δ^{18}O-CO_2 value at the North Pole of the standard run is in-between −1.3 and −1.4‰ but the Arctic-to-Antarctic difference goes down to −1.5‰ in the AR run. One can see in Figure 7b that all three extra processes of the standard run together reduce the north-south gradient by only about 0.1 to 0.2‰. The strongest influence is demonstrated by the ARMM and CA runs.

3.4.1.2. Monthly Mean Water Isotope Input

[31] ECHAM uses a soil bucket model for water as explained in part 1. So there is only one soil water content and one soil water δ^{18}O-H_2O. This simplification yields soil δ^{18}O-H_2O seasonal amplitudes that appear much too small (see part 1). δ^{18}O in CO_2 leaving the soil has thence almost the same value all yearlong in the model even if there is a major change in δ^{18}O-H_2O of incoming rain. In reality, δ^{18}O-H_2O at the soil surface changes considerably when it rains but this is attenuated in deeper soil so that δ^{18}O-H_2O of very deep soil does not change markedly [e.g., *Melayah et al.*, 1996]. The prevailing opinion is that δ^{18}O of CO_2

Table 2. Names and Contents of Sensitivity Runs[a]

Name	Ass	Resp	Oce	FF	BB	Inv	Carb. Anhy.	c_a Vari.	δ^{18}O Rain
AR	X	X							
AROCE	X	X	X						
ARFF	X	X		X					
ARBB	X	X			X				
ARINV	X	X				X			
ARCA	X	X					X		
ARCaVar	X	X						X	
ARMM	X	X							X
STD	X	X	X	X	X				
STDMM	X	X	X	X	X				X

[a]Ass stands for assimilation (A in name), Resp for respiration (R), Oce for the ocean exchange (OCE), FF for fossil fuel combustion (FF), BB for biomass burning (BB), Inv for the invasion effect (INV), Carb. Anhy. for reduced carbonic anhydrase activity (CA), c_a Vari. for variable atmospheric CO_2 mixing ratios in assimilation calculation (CaVar), and δ^{18}O Rain for monthly mean rain and vapor isotope input instead of δ^{18}O-H_2O online calculation (MM). The names are then composed of the letters in the parentheses.

leaving the soil is in isotopic equilibrium with soil water at about 15 cm depth [*Riley et al.*, 2002; *Miller et al.*, 1999]. δ^{18}O-H_2O at 15 cm depth does not track the whole range of δ^{18}O-H_2O of incoming rain but the variation is notably attenuated. Previous models of δ^{18}O-CO_2 used monthly rain and its isotope values as an approximation for the "correct" δ-value of equilibrating soil water [e.g., *Peylin et al.*, 1999]. δ^{18}O-H_2O in 15 cm depth will lie between the two extremes, rain and soil bucket respectively, most of the time but can reach much higher values during longer drought periods. However, these periods are also marked by reduced CO_2 production in soil and by roots due to the limitation of water. We conducted thus a sensitivity experiment where δ^{18}O-CO_2 fluxes of the standard run (STD) do not depend on the online calculated δ^{18}O-H_2O values but are rather prescribed to monthly means of δ^{18}O-H_2O rain of the standard model run (STDMM). We treat this sensitivity run in detail because it shows one of the largest influences on the north-south gradient of all sensitivity runs (see Figure 7). Figure 9 shows results of the STD and STDMM runs, displayed as difference between model and measurements at the stations and as north-south gradient. Monthly mean water isotope input does not change greatly the north-south gradient in δ^{18}O-CO_2. The spread in the differences between model and measurements is not reduced and the latitudinal mean over ocean grid cells changes only marginally. The north-south gradient exhibits only the annual

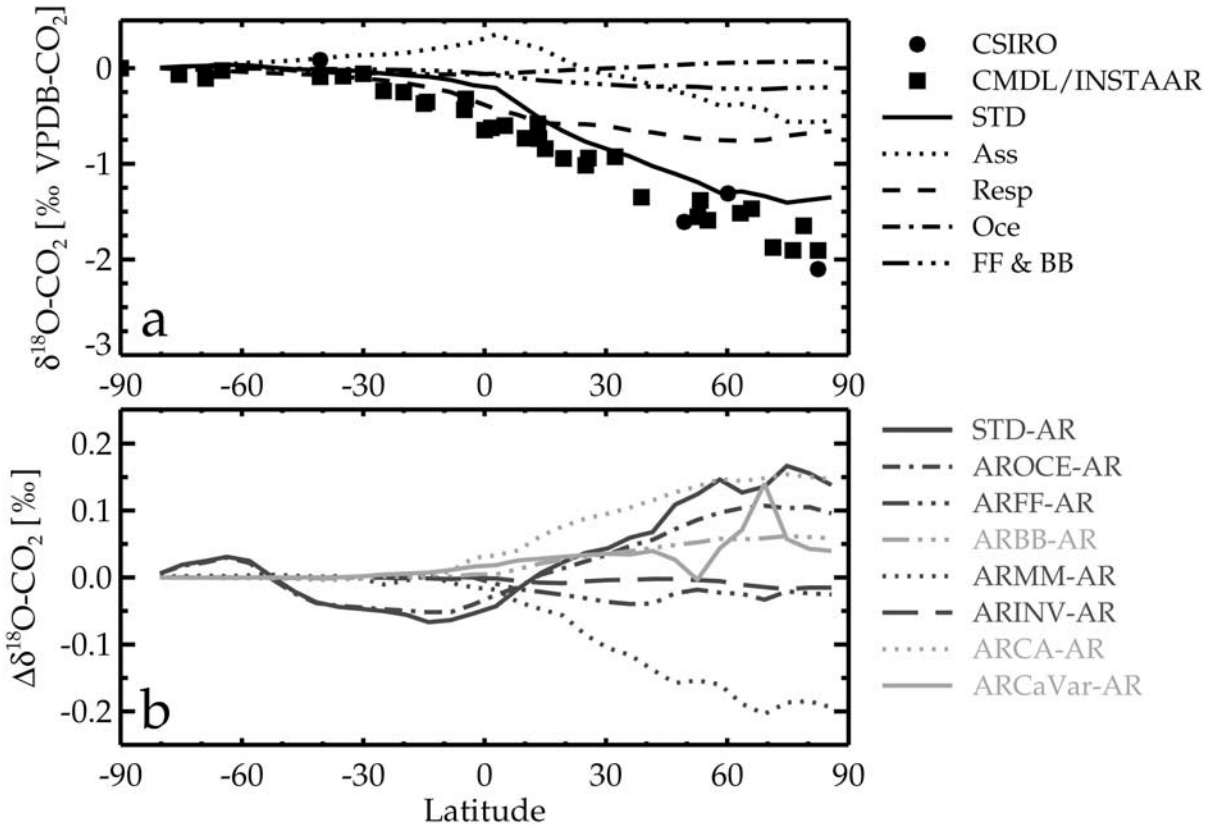

Figure 7. Contribution of different processes to the north-south gradient in δ^{18}O-CO_2. (a) The total north-south gradient of the standard run (STD) split up in the contributions of individual processes. The δ-anomalies are additive and sum up to the total signal so that adding up the different contributions at every latitude gives the total signal (solid line). Ass = contribution of assimilation, Resp = respiration, Oce = ocean, FF & and BB = fossil fuel and biomass burning. (b) The total north-south gradient signal of different runs, including a specific extra process, minus the north-south gradient of a run with only assimilation and respiration included (AR). The names of the runs are explained in Table 2, together with run descriptions.

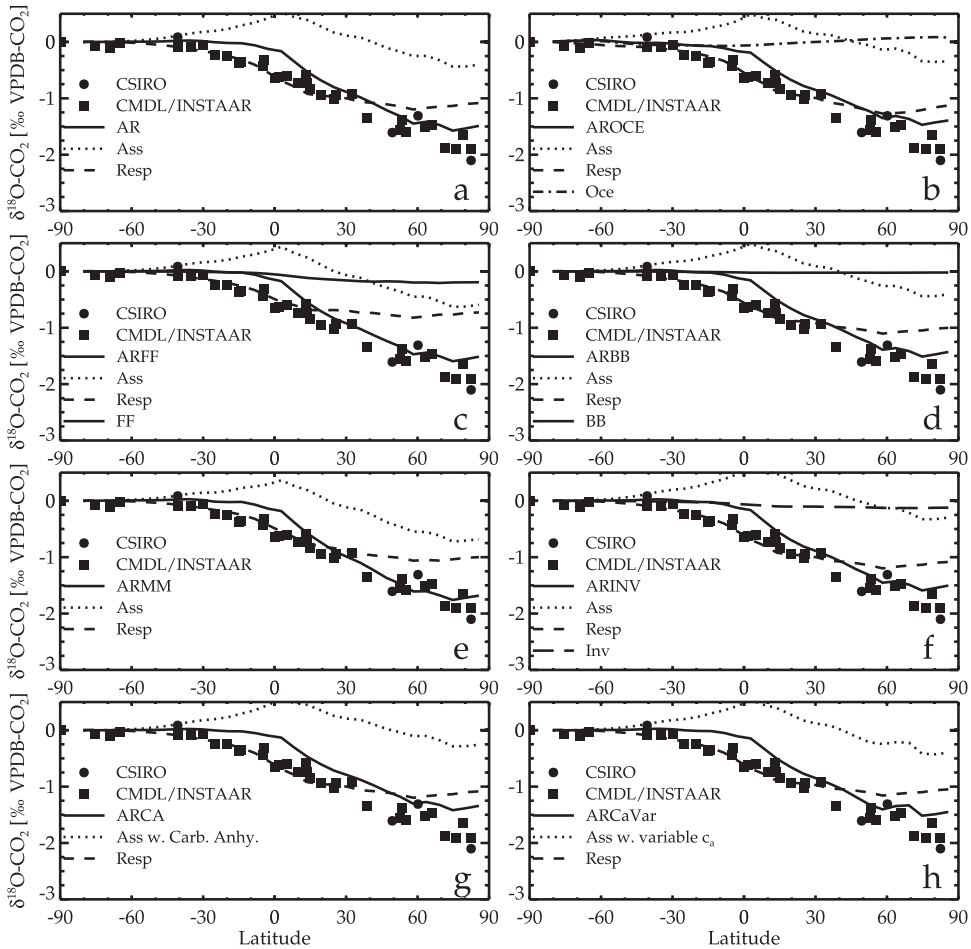

Figure 8. North-south gradient of all runs in Figure 7b split up in their individual processes. Figure 8a is the run with only assimilation and respiration, whose total δ^{18}O-CO_2 signal was subtracted in Figure 7b from the δ^{18}O-CO_2 north-south gradient of the different runs. Figures 8b–8h show runs identical to Figure 8a, but with one further process added in the calculation (names in Table 2). In Figure 8b, ocean CO_2 fluxes were added to assimilation and respiration fluxes, AROCE. In Figure 8c, fossil fuel combustion was added, ARFF; in Figure 8d, biomass burning fluxes were added, ARBB; in Figure 8e, δ^{18}O of water was prescribed to monthly means of δ^{18}O-H_2O rain of the standard run, ARMM; in Figure 8f, invasion was present in the model, ARINV; in Figure 8g, the activity of carbonic anhydrase were reduced, ARCA; and in Figure 8h, assimilation fluxes were calculated with instantaneous CO_2 mixing ratios of the lowest model layer, ARCaVar.

mean, also from the underlying source functions. The respiration-weighted annual mean of soil water isotopes did change but influenced both, assimilation and respiration. Together with the feedback of the atmospheric δ value on apparent discriminations, the influence of monthly mean water isotope input is cancelled almost completely.

3.4.1.3. Reduced Carbonic Anhydrase Activity

[32] As explained in part 1, the enzyme carbonic anhydrase, distributed in the mesophyll cells, speeds up the hydration of CO_2 by a factor 10^7 [*Stryer*, 1981]. CO_2 molecules entering the stomata are hence immediately hydrated even if they cannot be taken up by RUBISCO because of limitations of, e.g., electron transport (cf. part 1). If CO_2 molecules are not assimilated by the plant, they diffuse back in the stomata and subsequently into the canopy. However, once CO_2 molecules were hydrated in leaf water, they have most probably isotopically equilibrated with it and the back-diffused CO_2 molecules carry the leaf water isotopic signature in the atmosphere. If the activity of carbonic anhydrase is reduced, not all CO_2 molecules entering the stomata are hydrated before they diffuse back into the canopy [*Gillon and Yakir*, 2001]. This reduces leaf discrimination by only 1‰ in the global mean in our model and reduces hence the influence of assimilation on δ^{18}O of atmospheric CO_2. Lower stomata-internal CO_2 mixing ratios increase the effect of reduced carbonic anhydrase activity. We have high stomata-internal CO_2 mixing ratios (at least at high northern latitudes, see part 1) so that *Gillon and Yakir* [2001] estimate a greater global reduction of leaf discrimination of 2–3‰. However, this effect is of the same order of magnitude as the ARMM run and likewise its influence on the meridional gradient is negligible.

3.4.1.4. Other Processes

[33] To demonstrate the change of leaf discrimination and apparent soil discrimination due to different processes in more detail, we plot in Figure 8a the meridional gradient of

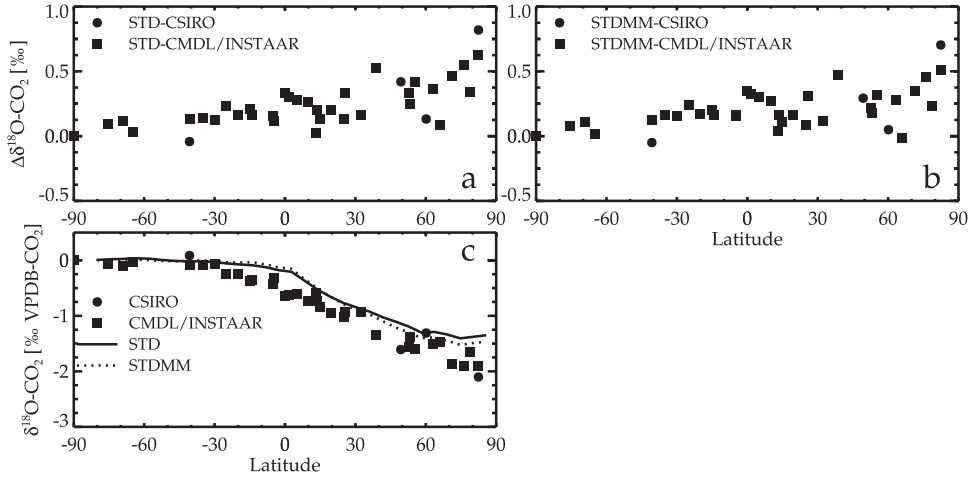

Figure 9. Meridional gradient of δ^{18}O-CO_2 relative to South Pole. (a) Difference between the model values at particular stations and the measurements at these stations. (b) Same as Figure 9a, but with a model run where the water isotopes are introduced as monthly mean rain and vapor isotope values. (c) Data and latitudinal mean over ocean grid cells of the standard run and the run with monthly mean water isotope input of Figure 9b. Note that Figure 9c represents the STDMM run and Figure 8e the ARMM run.

δ^{18}O-CO_2 of the AR run together with the individual contributions of assimilation and respiration. Figures 8b–8h show then the results of sensitivity runs where other processes are added to assimilation and respiration, namely the ocean fluxes, fossil fuel combustion, biomass burning, the isotopic water source as monthly mean input fields of rainwater isotopes, the invasion effect, the reduced carbonic anhydrase activity, and varying CO_2 concentrations in air, c_a. (Normally, c_a is fixed to 353 ppm in the calculation of assimilation in ECHAM/BETHY but not in the $C^{18}O$ flux calculations.). Comparing Figure 8a with Figure 8c shows the change in the model behavior due to fossil fuel combustion input. One can see in Figure 7b that the total meridional mean changes only little but Figures 8a and 8c show that the contributions of assimilation and respiration change considerably. Fossil fuel combustion adds about −0.2‰ to the total signal, assimilation changed also about −0.2‰ compared to the AR run but this is almost totally compensated for by the change in the respiration contribution of around +0.3 to 0.4‰. Monthly mean rain isotope input strengthens the influence of assimilation and weakens the respiration contribution (Figure 8e) whereas reduced carbonic anhydrase acts the other way round (Figure 8g), weakening assimilation influence and consequently strengthening respiration (δ_a is reduced because of reduced leaf discrimination that in turn reinforces the apparent soil discrimination). Figures 7b and 8f show that the "invasion effect" (explained in part 1) does not change markedly the meridional gradient. In further runs, we changed the fractionations, ϵ, applied to the different processes (as explained in part 1) but the interactively calculated apparent discriminations changed accordingly as demonstrated in Figure 8 so that we ended up always with a very similar picture (results not shown here). We also exchanged the global fractionations with parameterizations depending on climate and/or biospheric variables [e.g., *Ball*, 1987; *Farquhar and Lloyd*, 1993; *Roden and Ehleringer*, 1999; *White*, 1983] but the effect on the meridional gradient were again negligible (results not shown here).

[34] In summary, assimilation and respiration are the determining factors of the meridional gradient and because of interactively calculated apparent discriminations, none of the proposed processes helps to improve our modeling of the north-south gradient.

3.4.2. Sensitivity of δ^{18}O-CO_2 Seasonal Cycle

[35] The seasonal variations of the isofluxes alter the influence of individual processes with time. The seasonal cycle can be influenced by changes to model formulations even if the meridional gradient is not. We explain in this section the influence of different sensitivity tests on the seasonal cycle but do not plot the results because all of the performed sensitivity studies changed mainly the amplitude of the seasonal cycle and not significantly the phase. We diagnose the seasonal amplitude of δ^{18}O-CO_2 as somewhat adjustable and must resolve the phase mismatch between model and measurements first before we can find a feasible set of parameters for the amplitude.

[36] The ARMM and STDMM runs were explained in detail in the previous section. The water isotopic composition distribution is reflected in the north-south gradient mainly as a respiration weighted annual mean. However, the ARMM and STDMM runs differ from their 'parent' runs, with δ^{18}O-H_2O calculated online, stronger in the seasonal cycle than in the annual mean of δ^{18}O-H_2O. The phasing of the rainwater isotopes coincides with the phase of the CO_2 fluxes in our model so that the ARMM and STDMM runs did not significantly change the seasonal cycle of δ^{18}O-CO_2 (results not shown here). The evidence of reduced carbonic anhydrase activity leads to a different pattern in atmospheric δ^{18}O-CO_2. Carbonic anhydrase activity in C_3 plants is significantly less reduced than in C_4 plants, and we tested that this effect can substantially change the seasonal cycle at some stations because of a modified influence of assimilation on the total signal but it does not improve the phase mismatch between model and measurements. Predictably, other processes with no great seasonal variation, like fossil fuel combustion, had almost

no influence on the seasonal cycle of δ^{18}O-CO_2. Assimilation and respiration isofluxes changed when introducing these processes because of modified apparent discriminations caused by the feedback. These changes were very small, though. However, some seasonal processes missing in our model might influence δ^{18}O-CO_2. We confirmed that the ''invasion effect'' cannot be a significant influence (results not shown here; one can see the influence of invasion on the north-south gradient in Figure 8f, and it is very small there, the same is true for the seasonal cycle).

[37] It is very possible that the parameterizations used, comparable to *Ciais et al.* [1997a, 1997b], are not sufficient to describe the seasonal cycle of δ^{18}O-CO_2. Exchanging for example the global fractionations, ϵ, with parameterizations that depend on climate and/or biospheric variables (see previous section for citations) did change the amplitude and therefore the phase of the seasonal cycle of δ^{18}O-CO_2. The modified parameters sometimes changed the amplitude significantly, but not very much the phase. Sensitivity studies with different sets of global fractionation values showed the same behavior. Reducing for example the kinetic fractionation of δ^{18}O-CO_2 leaving the soil, thereby diminishes the influence of respiration on δ^{18}O-CO_2. Changing the fractionation in a reasonable range can amplify or divide the amplitude of the seasonal cycle by almost a factor of 1.5. However, the phase is not changed greatly.

[38] None of the tested processes and parameterizations resolved the mismatch between our model and the observations in either the north-south gradient or in the seasonal cycle. Although, we have changed biosphere apparent discriminations considerably, this did not greatly change the phasing of the seasonal cycle. Therefore either an important process is missing in the model, an included process is wrongly parameterized or the biosphere CO_2 gross fluxes are erroneous. The very good CO_2 seasonal cycle comparison argues against erroneous gross fluxes, even though a good comparison in CO_2 can be found with quite different flux patterns [*Kaminski et al.*, 2001]. From a mechanistic point of view, the weakest parameterization in our model is the formulation of the heterotrophic respiration because it is described with only a very simple formulation (see part 1). We use air temperature to parameterize heterotrophic respiration [*Raich and Potter*, 1995]. Using soil temperature instead [*Lloyd and Taylor*, 1994] changes the shape of heterotrophic respiration so that it peaks later in year. This test resulted in a convergence of model and observations in δ^{18}O-CO_2 but the model deviated from the observations in CO_2. This effect can be seen in the simulation of *Ciais et al.* [1997a, 1997b] and *Peylin et al.* [1999] who used monthly biosphere fluxes from the SIB2 biosphere model [*Denning et al.*, 1996a, 1996b] to compute δ^{18}O-CO_2. SIB2 shows the same phase in assimilation as BETHY but respiration has its maximum 1 to 2 month later in the extratropics (SIB2 uses soil temperature for heterotrophic respiration [*Denning et al.*, 1996a]). Therefore the simulations of Ciais et al. and Peylin et al. show δ^{18}O-CO_2 seasonal cycles closer to the measurements than ours in high latitudes but their simulated CO_2 seasonal cycle shows a phase shift compared to the observations. SIB2 and BETHY are very similar in the phase of respiration in the tropical region so that consequently the simulations of Ciais et al. and Peylin et al. show the same phase lag as ECHAM/BETHY in δ^{18}O-CO_2 at mid-latitudes whereas the CO_2 seasonal cycles match the phase of the observed cycles in both models.

4. Summary and Concluding Remarks

[39] We have built a detailed global 3-D model of δ^{18}O in atmospheric CO_2. The model simulates very well the seasonal cycle of CO_2 at atmosphere observatories, even though at 25% of the stations, ECHAM/BETHY fails to follow closely the seasonal cycle of CO_2 because of model deficiencies. This is mainly due to deficiencies in the AGCM ECHAM rather than in the biospheric part BETHY. ECHAM/BETHY shows a seasonal cycle of δ^{18}O in atmospheric CO_2 very similar to the cycle in CO_2, i.e., that CO_2 and δ^{18}O-CO_2 show their minimum and maximum at the same time. The modeled seasonal cycle of δ^{18}O-CO_2 precedes the measurements by two months at almost all stations. None of the sensitivity studies performed with ECHAM/BETHY did resolve this model shortcoming but did impact on the amplitude. Whereas the seasonal amplitude of δ^{18}O-CO_2 changes with different parameters or parameterizations up to a factor of 3, there is no significant effect on the phase. We think that it is always possible to find a reasonable set of parameters that fits the seasonal amplitude at most stations but consider it a futile exercise while the question of the phase mismatch is unresolved.

[40] The biosphere is set to equilibrium in our model, i.e., there is no annual mean net biosphere flux from any land point in the model. The annual mean net δ^{18}O-CO_2 isoflux is zero only in the global mean but imbalanced on every grid point. This yields a northern hemispheric isoflux of -160 GtC ‰ yr^{-1} which is balanced in the southern hemisphere by +160 GtC ‰ yr^{-1}. A first-order two box model such as that used in TRANSCOM phase 1 [*Law et al.*, 1996] relates concentration differences, c_-, with source strength differences, S_-:

$$c_- = \frac{\tau}{2} S_- \tag{6}$$

where τ is the interhemispheric exchange time. The range in τ in the models of TRANSCOM Phase 1 was roughly between 1 and 2 years (we did no experiment to determine τ in ECHAM). The source strength difference between northern and southern hemispheric δ^{18}O-CO_2 isofluxes yields therefore a concentration difference of -0.3 to -0.5‰ whereas the model shows a difference of about -0.6‰ in the lowest model layer over the ocean. The excess in the model comes from the rectifier effect, i.e., the covariance between the diurnal and seasonal cycle of δ^{18}O-CO_2 with transport. It has a much stronger impact on the north-south gradient than any other process in our model apart from assimilation and respiration.

[41] None of the sensitivity studies changed the gradient of δ^{18}O-CO_2 between Arctic and Antarctica by more than 10% neither did they change the phase of the modeled seasonal cycle of δ^{18}O-CO_2 significantly. We speculate five mechanisms which could be responsible for the mismatch:

[42] The first possible mechanism is the interfacing of BETHY and ECHAM. BETHY is interfaced to ECHAM rather than coupled. This means that BETHY is driven by ECHAM meteorological parameters but ECHAM itself is not influenced by BETHY. A real coupling of a biosphere

model with an AGCM would imply that the AGCM is influenced by the biosphere model, e.g., through albedo and evapotranspiration. Coupling BETHY with ECHAM could lead to quite different or only subtle CO_2 flux changes. It would also change the calculation of the water isotopic composition. This would influence CO_2 as well as δ^{18}O-CO_2 and it is not foreseeable if it would make the comparison better or worse.

[43] Second, the imbalance in the net δ^{18}O-CO_2 isoflux could be responsible for the mismatch. A mean τ of 1.5 years (assuming that the rectifier effect is correctly represented) implies that the imbalance should be greater by a factor of approximately 1.5, means $S_{-} = 480$ GtC ‰ yr^{-1}. This can be achieved in several ways and Figure 8e shows that a more varying rain isotope source points in the right direction. However, also a change in CO_2 fluxes can lead to another imbalance in the net δ^{18}O-CO_2 isoflux. We discussed in part 1 that ECHAM/BETHY feature low-CO_2 fluxes at high northern latitudes. Increasing assimilation and therefore the respiration in high northern latitudes yields a greater imbalance in δ^{18}O-CO_2 net isoflux. We discussed as well in part 1 that the accompanying stomata-internal CO_2 mixing ratios, c_i, of ECHAM/BETHY are higher than other estimates. However, reduced c_i (at high northern latitudes) would lead to a reduced imbalance between northern and southern hemisphere in the δ^{18}O-CO_2 net isoflux which causes our model to depart further from the observations.

[44] Third, the rectifier effect could be modeled erroneously. The covariance between the diurnal and seasonal cycle of δ^{18}O-CO_2 with transport is already very strong in our model and achieves a meridional gradient in CO_2 which is higher than all models in TRANSCOM Phase 1 except for the CSIRO model which is comparable to ECHAM/BETHY [*Law et al.*, 1996]. To bring modeled and observed north-south gradient in δ^{18}O-CO_2 closer together, the rectifier effect has to be even stronger as it already is in our model.

[45] The soil water isotopes are the fourth possibility that could lead to the described mismatch. The soil bucket model of ECHAM attenuates too much the seasonal cycle of δ^{18}O-H_2O of water in the unsaturated soil zone. Soil CO_2 efflux exhibits therefore almost the same δ^{18}O-CO_2 value all yearlong. The performed sensitivity analysis used monthly mean rain isotope input that coincided in its seasonal phasing with the seasonal phasing of assimilation in the model, so that no strong sensitivity could be observed. This could be an artefact due to the synchronous seasonal cycles. A more realistic formulation of the soil water profile like the one of *Riley et al.* [2002] leads to an integration of rainwater isotopes with higher seasonal variations than the soil bucket model. The integrated signal shows then a seasonal amplitude lagging the rain water isotope input, which would translate in a greater amplitude of the apparent soil discrimination and also in a different seasonal phasing of the apparent soil discrimination respectively soil isoflux.

[46] Fifth, the missing stratosphere-troposphere exchange (STE) of enriched δ^{18}O-CO_2 could ameliorate the comparison. *Gamo et al.* [1989] reported for the first time δ^{18}O-CO_2 values in the stratosphere that were enriched by 2 to 3‰ compared to tropospheric values. This is probably due to the isotopic exchange of CO_2 with ozone in the stratosphere [*Thiemens*, 1999] that is known to be highly enriched in ^{18}O [e.g., *Mauersberger*, 1981]. The exchange between troposphere and stratosphere has a strong seasonal cycle, is much bigger in the northern hemisphere than in the southern hemisphere, and has a maximum exchange in spring [*Zahn et al.*, 1999, 2000, and references therein]. Intrusion into the stratosphere passes mainly in the tropics whereas stratospheric air penetrates the troposphere in the extra-tropics contributing to a north-south gradient in δ^{18}O-CO_2 [*Peylin et al.*, 1997] and possibly to the seasonal cycle at tropospheric stations. Having 19 model levels, the representation of the stratosphere is very coarse in ECHAM so that STE exchange is not realistic [*Timmreck et al.*, 1999; *Kjellström et al.*, 2000]. We could therefore not include this process in our model and it is possible that the seasonal exchange of the STE changes the δ^{18}O-CO_2. However, the isotope enrichment of CO_2 in the lower stratosphere compared to the upper troposphere is only around 2‰. The box model of *Hesshaimer* [1997] estimates a gross STE CO_2 flux of 200 GtC yr^{-1} that yields an isoflux of about 400 GtC ‰ yr^{-1} which is of the order of magnitude of other processes like, e.g., fossil fuel combustion. However, the only δ^{18}O-CO_2 modeling study that includes the stratospheric enrichment [*Peylin et al.*, 1997] adapted a $CO^{18}O$ flux in the upper troposphere in order to match the measured profiles in δ^{18}O-CO_2 of *Gamo et al.* [1989] returning an isoflux of 200 GtC ‰ yr^{-1}. It is possible that the stratospheric enrichment plays its role in the δ^{18}O-CO_2 cycle but it is likely that the Arctic-to-Antarctic difference does not change significantly but behaves similar to the other sensitivity runs because of the interactive nature of the calculations. However, the STE is highest in spring and more pronounced in the extra-tropics. This could transport enriched δ^{18}O-CO_2 to tropospheric stations mainly in spring which could shift the maximum of the seasonal cycle and consequently the minimum, too.

[47] The atmospheric transport and the biospheric δ^{18}O-CO_2 fluxes determine almost completely the seasonal cycle and the north-south gradient of δ^{18}O in atmospheric CO_2. This underlines the high potential of δ^{18}O in atmospheric CO_2 to quantify the biospheric CO_2 gross fluxes, when δ^{18}O-CO_2 is eventually fully understood. If one controls the atmospheric transport, the atmospheric signal of δ^{18}O-CO_2 can thus be used to deduce CO_2 gross fluxes. Inversion techniques with global atmospheric transport models attempt this on a global scale [*Peylin*, 1999]. On a local scale, investigators handle the atmospheric transports either with transport tracers like ^{222}Radon [*Langendörfer et al.*, 2002] or with theoretical calculations [*Yakir and Wang*, 1996]. However, until now, no global study has been able to resolve the discrepancy between modeled and measured seasonal cycles of δ^{18}O-CO_2.

[48] **Acknowledgments.** We thank Ken Masarie for the support in processing the observational data. Computing facilities were provided by the Deutsche Klimarechenzentrum (DKRZ), Hamburg, Germany. M.C. was partially supported by the German Academic Exchange Office (DAAD), benefited from a travel grant of the Biosphere-Atmosphere Stable Isotope Network (BASIN), and had access to DKRZ facilities because of the support of the Max Planck Institute of Meteorology (MPI-MET), Hamburg. The authors thank Graham Farquhar and two anonymous reviewers for the detailed, very helpful comments.

References

Araújo, A. C., et al., Comparative measurements of carbon dioxide fluxes from two nearby towers in central Amazonian rainforest: The Manaus LBA site, *J. Geophys. Res.*, *107*(D20), 8090, doi:10.1029/2001JD000676, 2002.

Bakwin, P. S., P. P. Tans, D. F. Hurst, and C. Zhao, Determination of the isotopic $^{13}C/^{12}C$ discrimination by terrestrial biology from a global network of observations, *Global Biogeochem. Cycles*, *12*, 555–562, 1998.

Ball, J. T., Calculations related to gas exchange, in *Stomatal Function*, edited by E. Zeiger, G. D. Farquhar, and I. R. Cowan, pp. 445–476, Stanford Univ. Press, Stanford, Calif., 1987.

Bowling, D. R., A. A. Turnipseed, A. C. Delany, D. D. Baldocchi, J. P. Greenberg, and R. K. Monson, The use of relaxed eddy accumulation to measure biosphere-atmosphere exchange of isoprene and other trace gases, *Oecologia*, *116*, 306–315, 1998.

Boyer, J. S., S. C. Wong, and G. D. Farquhar, CO_2 and water vapor exchange across leaf cuticle (epidermis) at various water potentials, *Plant Physiol.*, *114*, 185–191, 1997.

Ciais, P., et al., A three-dimensional synthesis study of $\delta^{18}O$ in atmospheric CO_2: 1. Surface fluxes, *J. Geophys. Res.*, *102*, 5857–5872, 1997a.

Ciais, P., et al., A three-dimensional synthesis study of $\delta^{18}O$ in atmospheric CO_2: 2. Simulations with the TM2 transport model, *J. Geophys. Res.*, *102*, 5873–5883, 1997b.

Ciais, P., P. Peylin, and P. Bousquet, Regional biospheric carbon fluxes as inferred from atmospheric CO_2 measurements, *Ecol. Appl.*, *10*, 1574–1589, 2000.

Ciais, P., R. J. Francey, P. S. Bakwin, K. A. Masarie, and P. P. Tans, Atmospheric CO_2 and tracers measurements to monitor the carbon cycle and its future evolution, in *Sixth International Carbon Dioxide Conference: Extended Abstracts*, pp. 1–4, Organ. Comm. of the 6th Conf., Sendai, Japan, 2001.

Cuntz, M., P. Ciais, and G. Hoffmann, Modelling the continental effect of oxygen isotopes over Eurasia, *Tellus, Ser. B*, *54*, 895–909, 2002.

Cuntz, M., P. Ciais, G. Hoffmann, and W. Knorr, A comprehensive global three-dimensional model of $\delta^{18}O$ in atmospheric CO_2: 1. Validation of surface processes, *J. Geophys. Res.*, *108*, doi:10.1029/2002JD003153, in press, 2003.

Denning, A. S., I. Y. Fung, and D. A. Randall, Latitudinal gradient of atmospheric CO_2 due to seasonal exchange with land biota, *Nature*, *376*, 240–243, 1995.

Denning, A. S., G. J. Collatz, C. Zhang, D. A. Randall, J. A. Berry, P. J. Sellers, G. D. Colello, and D. A. Dazlich, Simulations of terrestrial carbon metabolism and atmospheric CO2 in a general circulation model, part 1: Surface carbon fluxes, *Tellus, Ser. B*, *48*, 521–542, 1996a.

Denning, A. S., D. A. Randall, G. J. Collatz, and P. J. Sellers, Simulations of terrestrial carbon metabolism and atmospheric CO_2 in a general circulation model, part 2: Simulated CO_2 concentrations, *Tellus, Ser. B*, *48*, 543–567, 1996b.

Farquhar, G. D., and J. Lloyd, Carbon and oxygen isotope effects in the exchange of carbon dioxide between terrestrial plants and the atmosphere, in *Stable Isotopes and Plant Carbon-Water Relations*, edited by J. R. Ehleringer, A. E. Hall, and G. D. Farquhar, pp. 47–70, Academic, San Diego, Calif., 1993.

Farquhar, G. D., K. T. Hubick, A. G. Condon, and R. A. Richards, Carbon isotope fractionation and plant water-use efficiency, in *Stable Isotopes in Ecological Research*, edited by P. W. Rundel, pp. 21–41, Springer-Verlag, New York, 1989.

Francey, R. J., and H. S. Goodman, The DAR stable isotope reference scale for CO_2, in *Baseline Atmospheric Program (Australia) 1986*, edited by B. W. Forgan and P. J. Fraser, pp. 40–46, Dep. of Admin. Serv., Bur. of Meteorol., Melbourne, Victoria, Australia, 1988.

Francey, R. J., and P. P. Tans, Latitudinal variation in oxygen-18 of atmospheric CO_2, *Nature*, *327*, 495–497, 1987.

Gamo, T., M. Tsutsumi, H. Sakai, T. Nakazawa, M. Tanaka, H. Honda, H. Kubo, and T. Itoh, Carbon and oxygen isotope ratios of carbon dioxide of a stratospheric profile over Japan, *Tellus, Ser. B*, *41*, 127–133, 1989.

Gemery, P. A., M. Trolier, and J. W. C. White, Oxygen isotopic exchange between carbon dioxide and water following atmospheric sampling using glass flasks, *J. Geophys. Res.*, *101*, 14,415–14,420, 1996.

Gillon, J., and D. Yakir, Influence of carbonic anhydrase activity in terrestrial vegetation on the ^{18}O content of atmospheric CO_2, *Science*, *291*, 2584–2587, 2001.

GLOBALVIEW-CO_2, *Cooperative Atmospheric Data Integration Project: Carbon Dioxide* [CD-ROM], Clim. Monit. and Diagnostics Lab., NOAA, Boulder, Colo., 2002.

Heimann, M., and C. D. Keeling, A three-dimentional model of atmospheric CO_2 transport based on observed winds: 2. Model description and simulated tracer experiments, in *Aspects of Climate Variability in the Pacific and the Western Americas*, *Geophys. Monogr. Ser.*, vol. 55, edited by D. H. Peterson, pp. 237–275, AGU, Washington, D. C., 1989.

Hesshaimer, V., Tracing the global carbon cycle with bomb radiocarbon, Ph.D. thesis, Univ. Heidelberg, Heidelberg, Germany, 1997.

Kaminski, T., M. Heimann, P. Peylin, P. Bousquet, and P. Ciais, Inverse modeling of atmospheric carbon dioxide fluxes, *Science*, *294*, 259, 2001.

Kjellström, E., J. Feichter, and G. Hoffmann, Transport of SF_6 and $^{14}CO_2$ in the atmospheric general circulation model ECHAM4, *Tellus, Ser. B*, *52*, 1–18, 2000.

Langendörfer, U., M. Cuntz, P. Ciais, P. Peylin, T. Bariac, I. Milyukova, O. Kolle, T. Naegler, and I. Levin, Modelling of biospheric CO_2 gross fluxes via oxygen isotopes in a spruce forest canopy: A ^{222}Rn calibrated box model approach, *Tellus, Ser. B*, *54*, 476–496, 2002.

Law, R. M., et al., Variations in modeled atmospheric transport of carbone dioxide and the consequences for CO_2 inversion, *Global Biogeochem. Cycles*, *10*, 783–796, 1996.

Levin, I., et al., Three years of trace gas observations over the eurosiberian domain derived from aircraft sampling: A concerted action, *Tellus, Ser. B*, *54*, 696–712, 2002.

Levin, I., et al., Eurosiberian carbonflux: CO_2 intercomparison, in *Report of the Eleventh WMO/IAEA Meeting of Experts on Carbon Dioxide Concentration and Related Tracer Measurement Techniques, Tokyo, 25.–28. Sep. 2001, WMO Tech. Doc. 1138*, edited by S. Toru, chap. 3.8, pp. 37–54, World Meteorol. Organ., Geneva, 2003.

Lloyd, J., and J. A. Taylor, On the temperature dependance of soil respiration, *Funct. Ecol.*, *8*, 315–323, 1994.

Mahowald, N. M., P. J. Rasch, and R. G. Prinn, Cumulus parameterizations in chemical transport models, *J. Geophys. Res.*, *100*, 26,173–26,189, 1995.

Masarie, K. A., et al., NOAA/CSIRO flask air intercomparison experiment: A strategy for directly assesing consistency among atmospheric measurements made by independent laboratories, *J. Geophys. Res.*, *106*, 20,445–20,464, 2001.

Mauersberger, K., Measurements of heavy ozone in the stratosphere, *Geophys. Res. Lett.*, *8*, 935–937, 1981.

Melayah, A., L. Bruckler, and T. Bariac, Modeling the transport of water stable isotopes in unsaturated soils under natural conditions: 2. Comparison with field experiments, *Water Resour. Res.*, *32*, 2055–2065, 1996.

Miller, J. B., D. Yakir, J. W. C. White, and P. P. Tans, Measurement of $^{18}O/^{16}O$ in the soil-atmosphere CO_2 flux, *Global Biogeochem. Cycles*, *13*, 761–774, 1999.

Peylin, P., The composition of ^{18}O in atmospheric CO_2: A new tracer to estimate global photosynthesis (in French), Ph.D. thesis, Univ. Paris VI, Pierre et Marie Curie, 1999.

Peylin, P., P. Ciais, P. P. Tans, K. Six, J. A. Berry, and A. S. Denning, ^{18}O in atmospheric CO_2 simulated by a 3-D transport model: A sensitivity study to vegetation and soil fractionation factors, *Phys. Chem. Earth*, *21*, 463–469, 1997.

Peylin, P., P. Ciais, A. S. Denning, P. P. Tans, J. A. Berry, and W. C. White, A three-dimensional study of $\delta^{18}O$ in atmospheric CO_2: Contribution of different land ecosystems, *Tellus, Ser. B*, *51*, 642–667, 1999.

Raich, J. W., and C. S. Potter, Global patterns of carbon dioxide emissions from soils, *Global Biogeochem. Cycles*, *9*, 23–36, 1995.

Ramonet, M., and P. Monfray, CO_2 baseline concept in 3-D atmospheric transport models, *Tellus, Ser. B*, *48*, 502–520, 1996.

Riley, W. J., C. J. Still, M. S. Torn, and J. A. Berry, A mechanistic model of $H_2{}^{18}O$ and $C^{18}OO$ fluxes between ecosystems and the atmosphere: Model description and sensitivity analyses, *Global Biogeochem. Cycles*, *16*, 1095–1108, 2002.

Roden, J. S., and J. R. Ehleringer, Observations of hydrogen and oxygen isotopes in leaf water confirm the Craig-Gordon model under wide-ranging environmental conditions, *Plant Physiol.*, *120*, 1165–1173, 1999.

Roeckner, E., K. Arpe, L. Bengtsson, M. Christoph, M. Clausen, L. Dümenil, M. Esch, M. Giorgetta, U. Schlese, and U. Schulzweida, The atmospheric general circulation model ECHAM-4: Model description and simulation of present-day climate, *Tech. Rep. 218*, Max-Planck-Inst. für Meteorol., Hamburg, Germany, 1996.

Schmidt, M., R. Graul, H. Sartorius, and I. Levin, Carbon dioxide and methane in continental Europe: A climatology, and $^{222}Radon$-based emission estimates, *Tellus, Ser. B*, *48*, 457–473, 1996.

Schmidt, M., R. Neubert, C. Facklam, R. Heinz, R. Weller, and I. Levin, Variability of CO_2 and its stable isotopes at Schauinsland (Germany) and Neumayer (Antarctica), in *Sixth International Carbon Dioxide Conference: Extended Abstracts*, pp. 116–119, Organ. Comm. of the 6th Conf., Sendai, Japan, 2001.

Schulze, E.-D., F. M. Kelliher, C. Lloyd, and R. Leuning, Relationships among maximum stomatal conductance, ecosystem surface conductance, carbon assimilation rate, and plant nitrogen nutrition: A global ecology scaling exercise, *Annu. Rev. Ecol. Syst.*, *25*, 629–660, 1994.

Stephens, B. B., S. C. Wofsy, R. F. Keeling, P. P. Tans, and M. J. Potosnak, The CO_2 budget and rectification airborne study: Strategies for measuring rectifiers and regional fluxes, in *Inverse Methods in Global Biogeochemical Cycles*, *Geophys. Monogr. Ser.*, vol. 114, edited by P. Kasibhatla et al., pp. 311–324, AGU, Washington, D. C., 1999.

Stryer, L., *Biochemistry*, W. H. Freeman, New York, 1981.

Tans, P. P., Oxygen isotopic equilibrium between carbon dioxide and water in soils, *Tellus, Ser. B*, *50*, 163–178, 1998. (Correction, *Tellus, Ser. B*, *50*, 400, 1998.)

Tans, P. P., I. Y. Fung, and T. Takahashi, Observational constraints on the global atmospheric carbon dioxide budget, *Science*, *247*, 1431–1438, 1990.

Taylor, J. A., Atmospheric mixing and the CO_2 seasonal cycle, *Geophys. Res. Lett.*, *25*, 4173–4176, 1998.

Thiemens, M. H., Mass-independent isotope effects in planetary atmospheres and the early solar system, *Science*, *283*, 341–345, 1999.

Timmreck, C., H.-F. Graf, and J. Feichter, Simulation of Mt. Pinatubo volcanic aerosol with the Hamburg climate model ECHAM4, *Theor. Appl. Climatol.*, *62*, 85–108, 1999.

Trolier, M., J. W. C. White, P. P. Tans, K. A. Massarie, and P. A. Gemery, Monitoring the isotopic composition of atmospheric CO_2: Measurements from the NOAA global air sampling network, *J. Geophys. Res.*, *101*, 25,897–25,916, 1996.

White, J. W. C., The climatic significance of D/H ratios in white pine in the northeastern United States, Ph.D. thesis, Columbia Univ., New York, 1983.

Yakir, D., and X.-F. Wang, Fluxes of CO_2 and water between terrestrial vegetation and the atmosphere estimated from isotope measurements, *Nature*, *380*, 515–517, 1996.

Zahn, A., R. Neubert, M. Maiss, and U. Platt, Fate of long-lived trace species near the northern hemispheric tropopause: Carbon dioxide, methane, ozone, and sulfur hexafluoride, *J. Geophys. Res.*, *104*, 13,923–13,942, 1999.

Zahn, A., R. Neubert, and U. Platt, Fate of long-lived trace species near the northern hemispheric tropopause: 2. Isotopic composition of carbon dioxide ($^{13}CO_2$, $^{14}CO_2$, and $C^{18}O^{16}O$), *J. Geophys. Res.*, *105*, 6719–6735, 2000.

C. E. Allison and R. J. Francey, Division of Atmospheric Research, Commonwealth Scientific and Industrial Research Organisation, PMB 1, Melbourne, Victoria 3195, Australia. (colin.allison@csiro.au; roger.francey@csiro.au)

P. Ciais, M. Cuntz, and G. Hoffmann, LSCE CEA Saclay, Bât 709, L'Orme des Merisiers, F-91191 Gif-sur-Yvette Cedex, France. (ciais@lsce.saclay.cea.fr; cuntz@lsce.saclay.cea.fr; hoffmann@lsce.saclay.cea.fr)

W. Knorr, Max-Planck-Institut für Biogeochemie, Carl-Zeiss-Promenade 10, D-07745 Jena, Germany. (wknorr@bgc-jena.mpg.de)

I. Levin, Institut für Umweltphysik, Universität Heidelberg, Building INF 366, D-69120 Heidelberg, Germany. (lv@uphys1.uphys.uni-heidelberg.de)

P. P. Tans, Climate Monitoring and Diagnostic Laboratory, NOAA, Mail Code R/E/CG1, 325 Broadway, Boulder, CO 80303, USA. (ptans@cmdl.noaa.gov)

J. W. C. White, Institute of Arctic and Alpine Research and Department of Geological Sciences, University of Colorado, 1560 30th Street, Boulder, CO 80304, USA. (james.white@colorado.edu)